

# Physical properties of distant red galaxies in the COSMOS/UltraVISTA field

Zhongyang MA

*Center for Astrophysics, University of Science and Technology of China, Hefei 230026, China;  
Key Laboratory for Research in Galaxies and Cosmology, CAS, Hefei 230026, China.*

*mzy@mail.ustc.edu.cn*

Guanwen FANG \*

*Institute for Astronomy and History of Science and Technology, Dali University, Dali 671003, China;  
Key Laboratory for Research in Galaxies and Cosmology, CAS, Hefei 230026, China.*

*wen@mail.ustc.edu.cn*

Xu KONG

*Center for Astrophysics, University of Science and Technology of China, Hefei 230026, China;  
Key Laboratory for Research in Galaxies and Cosmology, CAS, Hefei 230026, China.*

*xkong@ustc.edu.cn*

and

Lulu FAN

*Center for Astrophysics, University of Science and Technology of China, Hefei 230026, China;  
Key Laboratory for Research in Galaxies and Cosmology, CAS, Hefei 230026, China.*

(Received ; accepted )

## Abstract

We present a study on physical properties for a large distant red galaxy (DRG) sample, using the  $K$ -selected multi-band photometry catalog of the COSMOS/UltraVISTA field and the CANDELS NIR data. Our sample includes 4485 DRGs with  $(J - K)_{\text{AB}} > 1.16$  and  $K_{\text{AB}} < 23.4$  mag, and 132 DRGs have HST/WFC3 morphological measurements. The results of nonparametric measurements of DRG morphology are consistent with our rest-frame UVJ color classification: quiescent DRGs are generally compact while star-forming DRGs tend to have extended structures. We find the star formation rate (SFR) and the stellar mass of star-forming DRGs present tight “main sequence” relations in all redshift bins. Moreover, the specific SFR (sSFR) of DRGs increase with redshift in all stellar mass bins and DRGs with higher stellar masses generally have lower sSFRs, which indicates that galaxies were much more active on average in the past, and star formation contributes more to the mass growth of low-mass galaxies than to high-mass galaxies. The infrared (IR) derived SFR dominate the total SFR of DRGs which occupy the high-mass

range, implying that the  $J - K$  color criterion effectively selects massive and dusty galaxies. DRGs with higher  $M_*$  generally have redder  $(U - V)_{\text{rest}}$  colors, and the  $(U - V)_{\text{rest}}$  colors of DRGs become bluer at higher redshifts, suggesting high-mass galaxies have higher internal dust extinctions or older stellar ages and they evolve with time. Finally, we find that DRGs have different overlaps with EROs, BzKs, IEROs and high- $z$  ULIRGs indicating DRGs is not a special population and they can also be selected by other color criteria.

**Key words:** galaxies: evolution – galaxies: formation – galaxies: high-redshift – galaxies: structure

## 1. Introduction

The universe at high redshift looks very different from that at low redshift and local. At the epoch of  $z \sim 2$ , a large fraction of massive galaxies are still active, and their morphology are quite different from that of nearby galaxies (McCracken et al. 2010; Fang et al. 2012; Wang et al. 2012). In order to examine current theoretical models of galaxy formation and evolution, studies of galaxies over a wide range of lookback time are needed (Shapley 2011). Within the past decade, many novel techniques have been applied to assemble multi-wavelength observations of galaxies at this important epoch and significant progress has been made in our understanding of high-redshift galaxies (Steidel et al. 1996; Smail et al. 1997; Franx et al. 2003; Daddi et al. 2004; Gronwall et al. 2007; Yan et al. 2007; Dey et al. 2008; Dunne et al. 2009; Caputi et al. 2012; Arcila-Osejo & Sawicki 2013; Ilbert et al. 2013).

At early time, one method for selecting high-redshift galaxies is the Lyman break technique, which uses the significant break at  $912 \text{ \AA}$  in the galaxy rest-frame UV spectrum to select star-forming galaxies (so-called Lyman Break Galaxies, or LBGs), and was first applied at  $z \sim 3$  (Steidel et al. 1996). The LBGs are UV-bright star-forming galaxies and dominated by relatively low-mass systems ( $\sim 10^{10} M_\odot$ ). Consider that most of local elliptical and S0 galaxies commonly have stellar masses great than  $10^{11} M_\odot$ , the LBGs may not be the progenitors of these massive galaxies today (Conselice et al. 2007), and the Lyman break technique have missed a significant population of red massive galaxies at high redshift, such as distant red galaxies (DRGs) (Franx et al. 2003), BzKs (Daddi et al. 2004), ultraluminous infrared galaxies (ULIRGs) (Chapman et al. 2003), etc. As a supplement to these UV-bright LBGs, Franx et al. 2003 introduced a new photometric technique for selecting  $z > 2$  massive red galaxies. The relevant spectral break is the Balmer break at  $3650 \text{ \AA}$  which attributes to the spectral shape of young stars and the  $4000 \text{ \AA}$  break which is caused by the absorption of metals in old stars. Since these breaks shift into the  $J$  band at  $z \sim 2$ , a red  $J - K$  color is a simple and effective criterion

---

\* Guanwen Fang and Zhongyang Ma contributed equally to this work.

(Franx et al. 2003). They simulated the tracks in the  $J - K$  color versus redshift diagram with model spectra taken from Bruzual & Charlot 1993, and imposed a criterion  $(J - K)_{\text{Vega}} > 2.3$  for selecting galaxies at  $z > 2$  (so-called Distant Red Galaxies, or DRGs).

DRGs commonly have higher star formation rates (SFRs) ( $\sim 100 M_{\odot}/\text{yr}$ ) and more dust extinctions ( $A_V = 1 - 3$  mag) (Franx et al. 2003; Förster Schreiber et al. 2004; Papovich et al. 2005; Webb et al. 2006). The redshift distribution of DRGs is quite broad, and the  $(J - K)_{\text{Vega}} > 2.3$  selection criterion does not uniquely sample high-mass galaxies (Papovich et al. 2005; Grazian et al. 2006; Conselice et al. 2007). However, DRG selection technique does locate very massive galaxies ( $\sim 10^{11-12} M_{\odot}$ ) at  $z > 2$  (van Dokkum et al. 2006; Conselice et al. 2007). In the present-day Universe, most of massive ( $M_* > 10^{11} M_{\odot}$ ) galaxies are quiescent systems. On the contrary, at  $z \sim 2$  a large proportion of massive galaxies are still active, while others are “red and dead” with little or no ongoing star-forming activities (Labbé et al. 2005; Papovich et al. 2006; Daddi et al. 2007; Wang et al. 2012). Transformation from the active systems into the evolved systems is a reasonable explanation to this dramatic evolution. Some studies suggested that DRGs show properties of both passive systems and dust obscured active systems (Förster Schreiber et al. 2004; Labbé et al. 2005; Papovich et al. 2005; Webb et al. 2006). Labbé et al. 2005 showed color tracks for stellar population models (Bruzual & Charlot 2003) in the  $(I - K)$  vs.  $(K - [4.5])$  diagram, and found that 70% of DRGs are well fit with dusty star-forming models and 30% are best described by old stellar population models. Webb et al. 2006 combined Spitzer  $24\mu\text{m}$  flux, and found a similar percentage ( $\sim 65\%$ ) of DRGs are dusty active galaxies. By studying the spectra, Kriek et al. 2006a; Kriek et al. 2006b found that the stellar populations differ greatly among DRGs, from dusty starburst with small break to evolved galaxy with strong break and no line emission, and both the  $\text{H}\alpha$  measurements and stellar continuum modeling imply 45% of  $K$ -selected massive galaxies at  $z \sim 2$  are not forming stars intensely.

The morphologies of DRGs are diverse. Toft et al. 2005 analyzed the morphologies of DRGs in the Hubble Ultra Deep Field based on HST Advanced Camera for Surveys (ACS) images and Near Infrared Camera and Multi-Object Spectrometer (NICMOS) images, and found that the rest-frame optical morphology of DRG is quite different from the rest-frame UV morphology. In the near-infrared images, some DRGs are extended and others are compact. Conselice et al. 2007 examined the morphologies of DRGs in the Extended Groth Strip (EGS) field based on ACS F814W images with eye-ball and nonparametric classification method, and found that the morphologies of DRGs show a diversity of types at all redshifts, from elliptical, peculiar to disk.

The  $(J - K)_{\text{Vega}} > 2.3$  criteria is a simple but outstanding selection method utilising the 3650 and 4000 Å breaks for high- $z$  massive red galaxies, which are supplements to those UV-bright low-mass LBGs. The DRG sample provides us with the chance to investigate the nature of the population of the massive red objects at high redshifts, which are supposed to be

the progenitors of local massive populations, thus it makes us better understand the evolution of massive galaxies. Since the DRG samples of previous research programs are commonly small ( $< 1000$ ), it still remains many uncertainties on the physical properties of distant red galaxies. In order to have a thorough understanding of this kind of galaxies, in this paper we present the largest sample of DRGs so far, which is selected from the COSMOS/UltraVISTA field, based on the high quality NIR data presented by McCracken et al. 2012 and Muzzin et al. 2013a. To clearly describe the details of the characteristics of DRGs, we investigate the correlations between their SFRs, redshifts, masses and morphologies. The rest-frame UV emission of galaxies is mainly contributed by the hottest stars and can be severely affected by dust extinction, therefore it is essential to study  $z \sim 2$  galaxies from observed NIR bands, which probe the rest-frame optical morphologies. Our morphology analysis was enabled by the HST Wide Field Camera 3 (WFC3) NIR imaging of the Cosmic Assembly Near-infrared Deep Extragalactic Legacy Survey (CANDELS)(Grogin et al. 2011; Koekemoer et al. 2011), and we compare the nonparametric measure of galaxy morphology with visual inspection and UVJ color-color diagram. In the meanwhile, we also compare DRG with other color selection criteria.

The paper is organized as follows. We introduce the  $K$ -selected catalog of the COSMOS/UltraVISTA field in Section 2, and the DRG sample selection method and classification in Section 3. We show our results on physical properties of DRGs in Section 4. We compare the DRG method with other color selection methods in Section 5, and conclude our results in Section 6. Throughout this paper, we assume an  $\Omega_M = 0.3, \Omega_\Lambda = 0.7$  and  $H_0 = 70$  km s $^{-1}$  Mpc $^{-1}$  cosmology, and all magnitudes and colors are given in AB system unless stated otherwise. Symbol such as “[3.6]” means the AB magnitude at the wavelength 3.6  $\mu$ m.

## 2. Observations and data

The COSMOS field is centered at  $\alpha = 10^h00^m28.6^s$ ,  $\delta = +02^d12^m21^s$  (J2000.0), and covers an area of  $\sim 2$  square degree (Scoville et al. 2007). The COSMOS project gathers a variety of ground- and space-based observations, covering nearly the whole spectrum range (Martin et al. 2005; Capak et al. 2007; Hasinger et al. 2007; Sanders et al. 2007; Schinnerer et al. 2007; Taniguchi et al. 2007; Lilly et al. 2009; Ilbert et al. 2010; McCracken et al. 2010).

The multi-band photometry data we used in this paper come from the  $K$ -selected catalog of the COSMOS/UltraVISTA field provided by Muzzin et al. 2013a, which is produced based on the near infrared (NIR) data from the UltraVISTA data release 1 (McCracken et al. 2012). The high-quality and deep-enough NIR data make it possible for us to select a large sample of DRGs. The catalog contains PSF-matched photometry in 30 photometric bands covering the wavelength from 0.15 $\mu$ m to 24 $\mu$ m, and includes the available GALEX (Martin et al. 2005), CFHT/Subaru (Capak et al. 2007), UltraVISTA (McCracken et al. 2012), S-COSMOS (Sanders et al. 2007), and zCOSMOS (Lilly et al. 2009) datasets. After removing regions contaminated

by bright stars, the effective area of overlap between optical and NIR data is  $1.62 \text{ deg}^2$ . The photometry in all bands is corrected for Galactic dust attenuation, and stars are separated from galaxies using the  $(J - K)$  vs.  $(u - J)$  color space, and it agrees well with `SExtractor`'s `class_star` parameters. The catalog is presented as a set of fluxes in the  $2''.1$  color aperture with an AB zeropoint of 25.0, and the 90% completeness limit of the catalog is  $K_{s,\text{tot}} = 23.4$ .

The derived physical parameters we used in this paper also come from the catalog provided by Muzzin et al. 2013a. Photometric redshifts are derived for all galaxies using the `EAZY` code (Brammer et al. 2008) with 30 bands, and have been calibrated by the highest-quality spectroscopic redshifts from zCOSMOS. The stellar population parameters such as stellar mass ( $M_*$ ), age,  $A_V$ ,  $\text{SFR}_{\text{SED}}$  are derived by SED fitting method in `FAST` code (Kriek et al. 2009a). The rest-frame UV luminosity is derived by `EAZY`. **The total IR luminosity is derived by fitting the  $24\mu\text{m}$  flux using the log-average of the Dale & Helou 2002 templates, but note that using the log-average of the Chary & Elbaz 2001 templates would provide very similar results.** Then the rest-frame UV and the total IR luminosities are converted to  $\text{SFR}_{\text{UV,uncorr}}$  and  $\text{SFR}_{\text{IR}}$  according to Kennicutt 1998. The total star formation rate of the galaxy can then be determined via  $\text{SFR}_{\text{tot}} = \text{SFR}_{\text{UV,uncorr}} + \text{SFR}_{\text{IR}}$ . The rest-frame  $U - V$  and  $V - J$  colors are calculated for all galaxies by `EAZY`, which determines the colors by integrating the best-fit SED through the redshifted filter curves over the appropriate wavelength range.

### 3. Selection and classification of DRGs

#### 3.1. DRG Sample Selection

To select a sample of DRGs from UltraVISTA catalog, firstly we remove all the objects classified as stars and contaminated galaxies defined by Muzzin et al. 2013a. In order to make our photometric selecting criterion close to the original DRG selecting criterion introduced by Franx et al. 2003, we make a simulation in BC03 code (Bruzual & Charlot 2003) to determine the corrections for  $J$  and  $K$  bands. Finally, we set a small correction for  $J - K$  color:  $(J - K)_{\text{UltraVISTA}} + 0.14 = (J - K)_{\text{ISAAC}}$  (AB), so we set  $(J - K)_{\text{UltraVISTA}} > 1.16$  (AB), which is equivalent to  $(J - K)_{\text{ISAAC}} > 1.3$  (AB), as the criterion for selecting DRGs. On the other hand, we carefully compared the location of the stellar sequence with previous works, and find the distance on  $J - K$  color between stellar sequence and DRG selecting criterion is 1.36, which is consistent with previous works (Foucaud et al. 2007; Kajisawa et al. 2008).

Figure 1 shows the  $K$ -selected galaxies (objects in masked area are removed) in the  $(J - K)$  vs.  $K$  diagram, the dashed line represents  $J - K = 1.16$ , which is our DRG selecting criterion, objects above which are all DRGs and are plotted in red color. The dot-dashed line represents the stellar sequence, and all stars are plotted in green color. The total number of DRGs we select from the COSMOS/UltraVISTA field is 4485 with  $K < 23.4$  and  $J < 24.2 \text{ mag}$



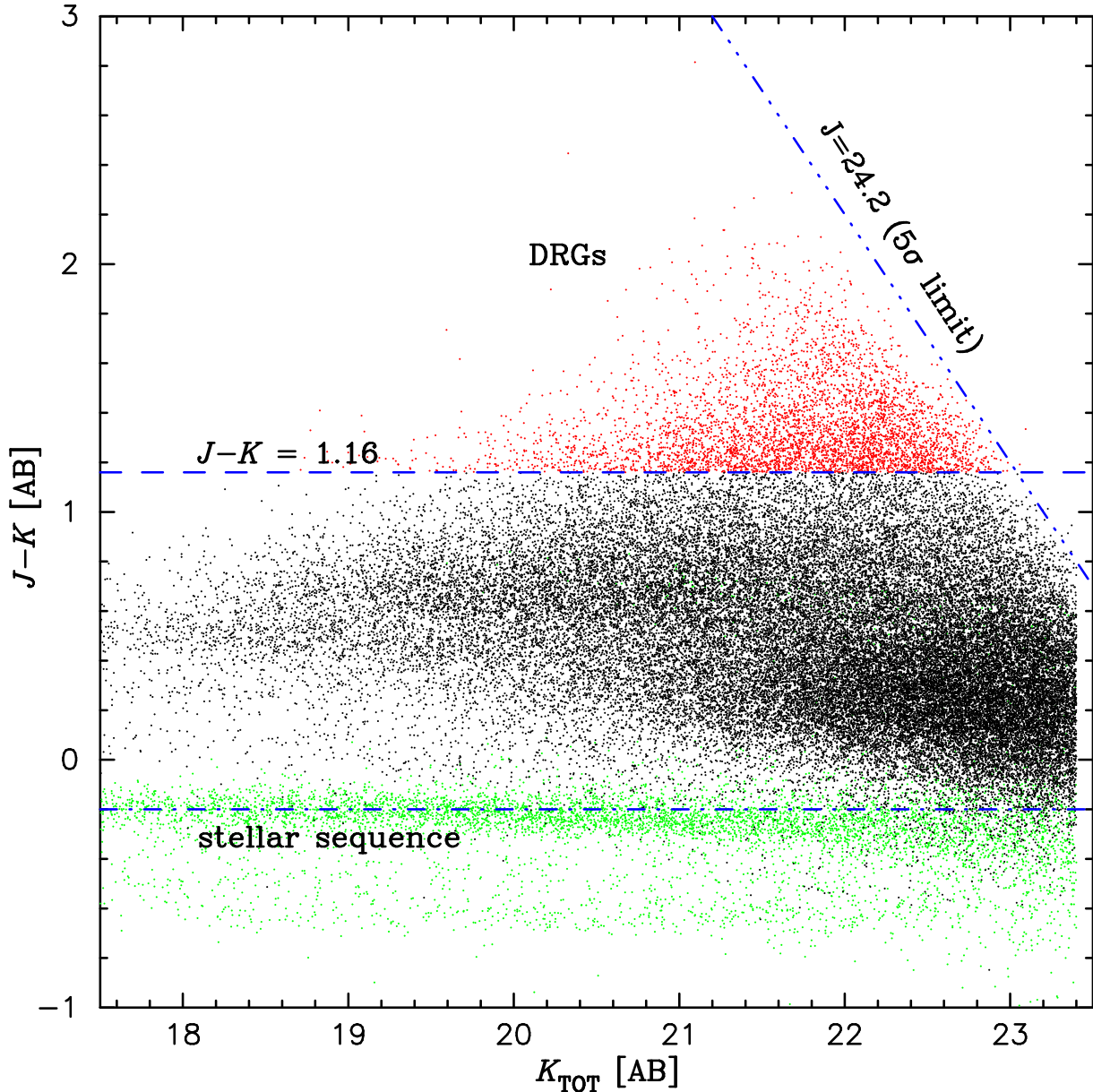


**Fig. 1.**  $(J - K)$  color vs.  $K$  magnitude for galaxies in the COSMOS/UltraVISTA field. The dashed line corresponds to  $J - K = 1.16$  which is our DRG selecting criterion, galaxies above which are all DRGs and are plotted in red color. The dot-dashed line represents the stellar sequence, and stars are plotted in green. The dot-dot-dashed line indicates the depth of the  $J$  band.

(Therefore, all DRGs in our sample actually have  $K < 24.2 - 1.16 = 23.04$  mag).

Figure 2 shows the  $K$ -band differential number counts of DRGs and all  $K$ -selected galaxies. For comparison, we have also plotted the number count results from other literature. In this figure, the red squares and the black triangles represent the number counts of DRGs and all  $K$ -selected galaxies in the COSMOS/UltraVISTA field, respectively. The blue stars represent the number counts of DRGs whose  $J$ -band magnitude limit is not considered. Results of DRGs from GOODS-S (Grazian et al. 2006), HDF-S (Labbé et al. 2003), GOODS-N (Kajisawa et al.

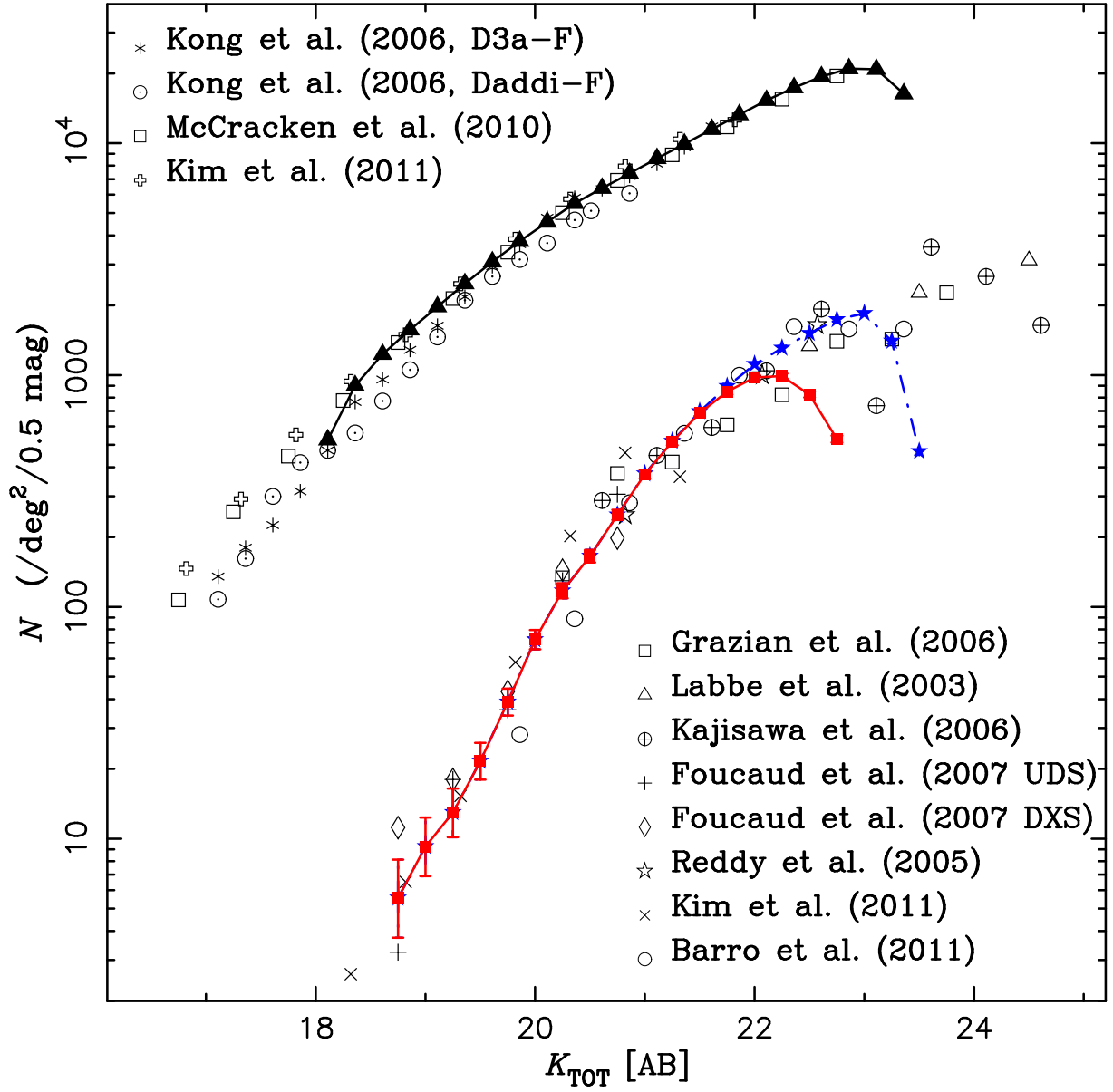


**Fig. 2.**  $K$ -band differential number counts for DRGs (red squares) and all  $K$ -selected galaxies (black triangles) in the COSMOS/UltraVISTA field. The blue stars represent the number counts of DRGs regardless of their  $5\sigma$  detection in  $J$ -band or lack thereof. For comparison, we also overplot the number counts of DRGs and all  $K$ -selected galaxies from previous works.

2006), UDS-EDR & DXS-EDR (Foucaud et al. 2007), GOODS-N (Reddy et al. 2005), UKIDSS (Kim et al. 2011) and EGS (Barro et al. 2011) are also plotted. And results of all  $K$ -selected galaxies from Deep3a-F & Daddi-F (Kong et al. 2006), COSMOS (McCracken et al. 2010) and UKIDSS (Kim et al. 2011) are plotted in different symbols as well. As shown by this figure, our number counts of DRGs and all  $K$ -selected galaxies in the COSMOS/UltraVISTA field are in good agreement with those in previous works in other fields.

### 3.2. Classification based on rest-frame UVJ colors

As shown by previous literatures (Labbé et al. 2005; Webb et al. 2006; Kriek et al. 2006a; Kriek et al. 2006b), DRG is a diverse population, most of the DRGs are dusty star-forming galaxies while others are old and red with little on going star formation activities. In order to specify the details of the physical properties and the evolution of them, separating DRGs into star-forming and quiescent populations is necessary.

We classify our sample as star-forming DRGs (sDRGs) and quiescent DRGs (qDRGs) based on the rest-frame UVJ color criteria defined by Muzzin et al. 2013b. According to their definition, qDRGs are classified by:

$$U - V > 1.3, V - J < 1.5, [\text{all redshifts}], \quad (1)$$

$$U - V > (V - J) \times 0.88 + 0.69, [0.0 < z < 1.0], \quad (2)$$

$$U - V > (V - J) \times 0.88 + 0.59, [1.0 < z < 4.0]. \quad (3)$$

Otherwise, they are star-forming DRGs. These classification criteria are plotted as dashed lines in Figure 3. Based on this classification method, we identify 3725 sDRGs and 760 qDRGs, the percentage of sDRGs is 83%, which is a little higher than previous results (Labbé et al. 2005; Webb et al. 2006).

### 3.3. Classification based on visual morphologies

Morphologies of DRGs provide direct information on the formation and evolution history of these objects, and correlate a range of physical properties such as stellar mass, SFR and rest-frame color. It is difficult to study morphologies of high redshift dusty galaxies based on their observed optical images, because their observed optical light probes the rest-frame UV emission for objects at  $z \sim 2$ , and their apparent morphologies can be easily changed by patchy dust extinction. For example, Conselice et al. 2007 showed that DRGs have peculiar, clumpy morphologies in the *HST*/ACS F814W band image. Based on the *HST* NICMOS-*JH* (0.''09/pixel) and ACS-*BViz* (0.''03/pixel) images, however, Toft et al. 2005 found that the rest-frame optical morphology of DRGs is quite different from the rest-frame UV morphology. The rest-frame UV emission of galaxies mainly contributed by the hottest stars and can be severely affected by dust extinction, therefore it is essential to study  $z \sim 2$  galaxies from observed NIR bands which probe the rest-frame optical morphologies. Our morphology analysis was enabled by the *HST*/WFC3 NIR imaging with a resolution of 0.''06/pixel from the Cosmic Assembly



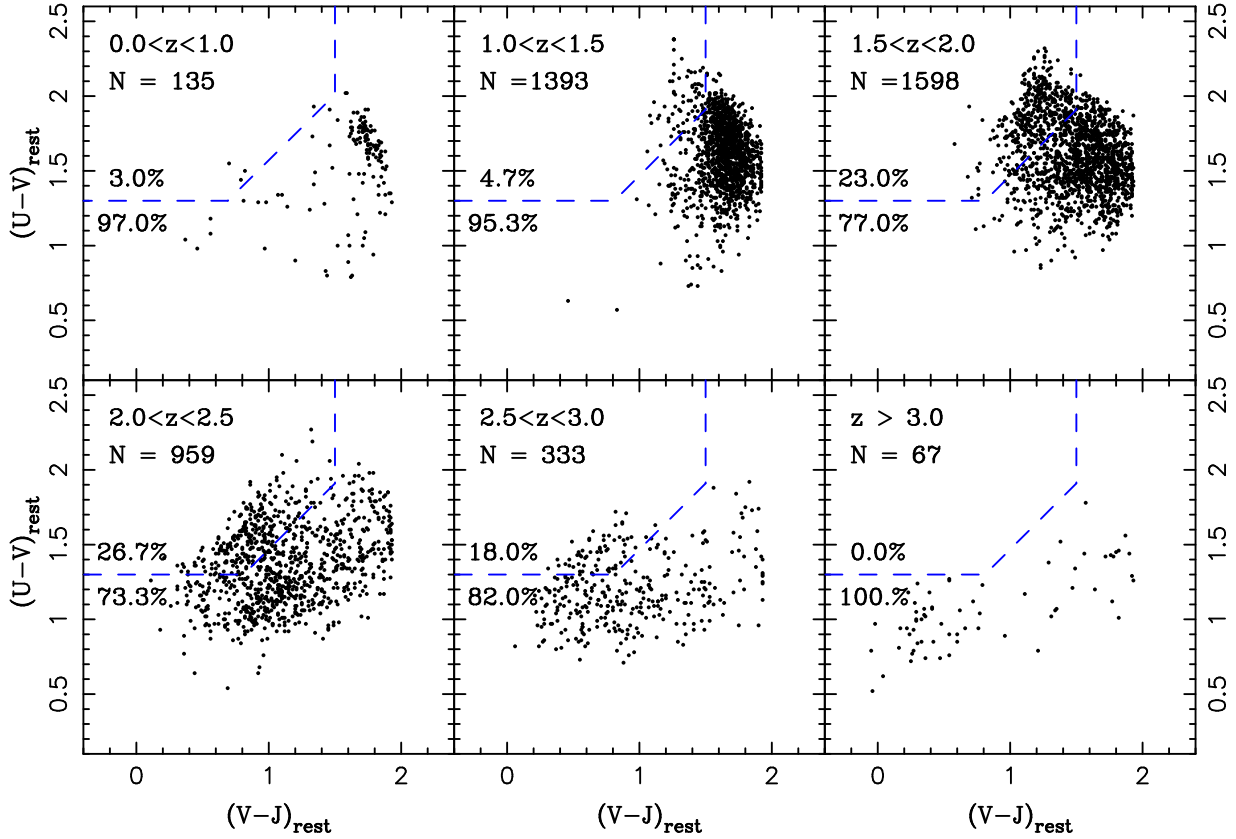


**Fig. 3.** Classification for DRGs based on rest-frame  $(U - V)$  vs.  $(V - J)$  colors in six redshift bins. This color criteria (dashed lines) used to separate star forming DRGs (sDRGs) and quiescent DRGs (qDRGs) are defined by Muzzin et al. 2013b. The number of DRGs, the fraction of sDRGs and qDRGs in each redshift bins are shown, respectively.

Near-infrared Deep Extragalactic Legacy Survey (CANDELS) (Grogin et al. 2011; Koekemoer et al. 2011).

Since the redshift distribution of DRGs is quite broad, we analyze their rest-frame optical morphologies on WFC3 F125W ( $J$ ) or F160W ( $H$ ) bands according to their redshifts. For DRGs with  $1 < z < 1.6$ , we choose WFC3 F125W ( $J$ ) bandpass for morphological analysis, it corresponds approximately to  $V$ -band in the rest-frame in this redshift range, but in the redshift range of  $1.6 < z < 3$ , we analyze galaxy morphology in the rest-frame  $V$  from the F160W ( $H$ ) image instead. Finally, 37 DRGs in our sample have  $J$ -band counterparts ( $1 < z < 1.6$ ), and 95 DRGs ( $1.6 < z < 3$ ) are detected at  $H$ -band image. The sensitivity ( $5\sigma$ ) of the CANDELS imaging data reach 27 mag in the F125W and the F160W, and all of DRGs in our sample are brighter than 24 mag in both  $J$  and  $H$  bands, thus the CANDELS data is deep enough to morphologically classify this DRG sample.

We perform the visual inspection for this sample by three of us independently, we combined each classifier's results and review the images together to resolve the disagreements. The disagreements cover about 10% of this sample, and mainly exist among galaxies which can't

**Table 1.** Numbers of star-forming and quiescent DRGs, classified by rest-frame UVJ colors in three visual morphological types.

DRGs ( $1 < z < 3$ )	Spheroid	Disk	Irregular	Total
Star-forming DRGs (sDRGs)	20	33	48	101
Quiescent DRGs (qDRGs)	24	5	2	31

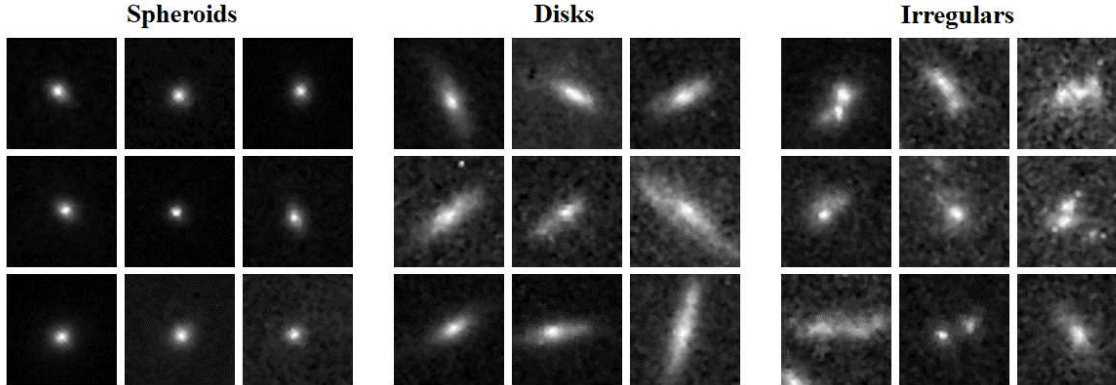


**Fig. 4.** Examples of three general morphological types from visual inspection: spheroid on the left, disk in the middle and irregular on the right panel. The size of each image is  $2''.4 \times 2''.4$ .

be clearly classified as disks or irregular galaxies. We find that the DRGs in our sample show very diversified morphologies, covering a wide range of types from extended disks, compact spheroids to clumpy and irregular morphologies. We define three general morphological types as follows:

**Spheroid** : round and centrally concentrated source with no extended structure.

**Disk** : single bright core with smooth extended disk-like structure.

**Irregular** : clumpy structure with more than two bright cores, sometimes shows interaction features such as tidal arms.

Examples of three morphological types are shown in Figure 4. The result of the visual inspection supports the finding that the significant evolution of the Hubble sequence has already existed at high redshift (Kajisawa & Yamada 2001). In Table 1 we list the numbers of star-forming and quiescent DRGs classified by rest-frame UVJ colors in three visual morphological types. Among star-forming DRGs, the spheroids occupy a proportion of 19.8%, disks occupy 32.7% and irregulars make up 47.5%. And among quiescent DRGs, the spheroids make up 77.4%, disks make up 16.1% and irregulars make up 6.5%. We find that most of quiescent DRGs are compact and star-forming DRGs tend to have extended structures.

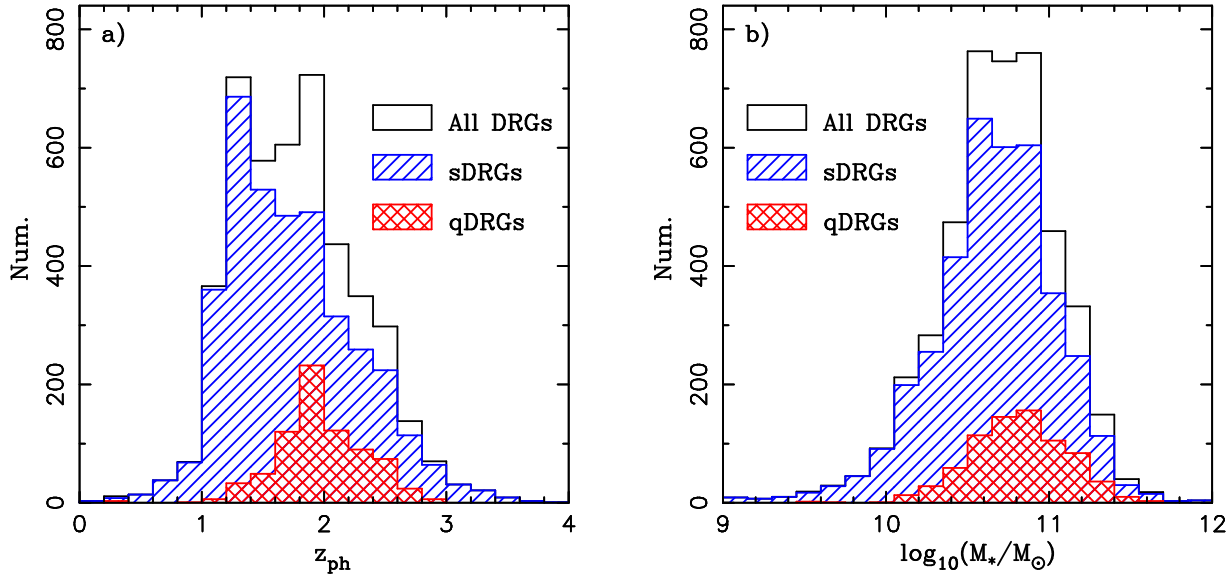


**Fig. 5.** Photometric redshift distribution (left panel) and stellar mass distribution (right panel) of DRGs. All DRGs are plotted in black lines, while star-forming and quiescent DRGs classified by rest-frame UVJ color are plotted in blue and red, respectively.

## 4. Results

### 4.1. Redshift and mass distributions

The photometric redshifts from the UltraVISTA catalog are in good agreement with the spectroscopic redshifts from zCOSMOS (Lilly et al. 2009), with an average  $\delta z/(1+z) = 0.013$  (Muzzin et al. 2013a). We show the redshift distributions of both star-forming and quiescent DRGs in the left panel of Figure 5. The star-forming DRGs (blue lines) distribute at  $0 < z < 3.5$  with  $\langle z \rangle = 1.74$ , and the quiescent DRGs (red lines) are in the range  $z \sim 1 - 3$  with  $\langle z \rangle = 1.98$ . For all DRGs, our sample has  $\langle z \rangle = 1.79$ . In total, there are 3% DRGs distribute at  $z < 1$ , 95.5% at  $1 < z < 3$  and 1.5% at  $z > 3$ . The right panel of Figure 5 shows the stellar mass distributions of both star-forming and quiescent DRGs. We find the masses of them are relatively high, and mainly range from  $10^{10} M_{\odot}$  to  $10^{11.5} M_{\odot}$ . The mean stellar masses are  $10^{10.7} M_{\odot}$ ,  $10^{10.6} M_{\odot}$  and  $10^{10.8} M_{\odot}$  for all, star-forming and quiescent DRGs in our sample, respectively.

We compare the redshift distributions of DRGs with those of all of galaxies in four stellar mass bins in Figure 6. We find that in higher mass bins (e.g.,  $10^{10.5} M_{\odot} - 10^{11} M_{\odot}$ ,  $10^{11} M_{\odot} - 10^{12} M_{\odot}$ ), DRGs represent nearly all of galaxies at  $z > 2$ . At  $M_* > 10^{10.5} M_{\odot}$  and  $z > 2$ , the fraction of DRGs out of all galaxies is 70%, which is in good agreement with van Dokkum et al. 2006. From the analysis above, we demonstrate that although DRG selecting criterion also sample low-mass galaxies at low redshifts, DRGs occupy large proportion of galaxies at high-mass and high- $z$  range, implying that DRG selecting criterion is sensitive to massive galaxies at high redshifts. Our results are also demonstrated in Conselice et al. 2007. The spectroscopy study of Kriek et al. 2008 also supports our finding that red galaxies dominate

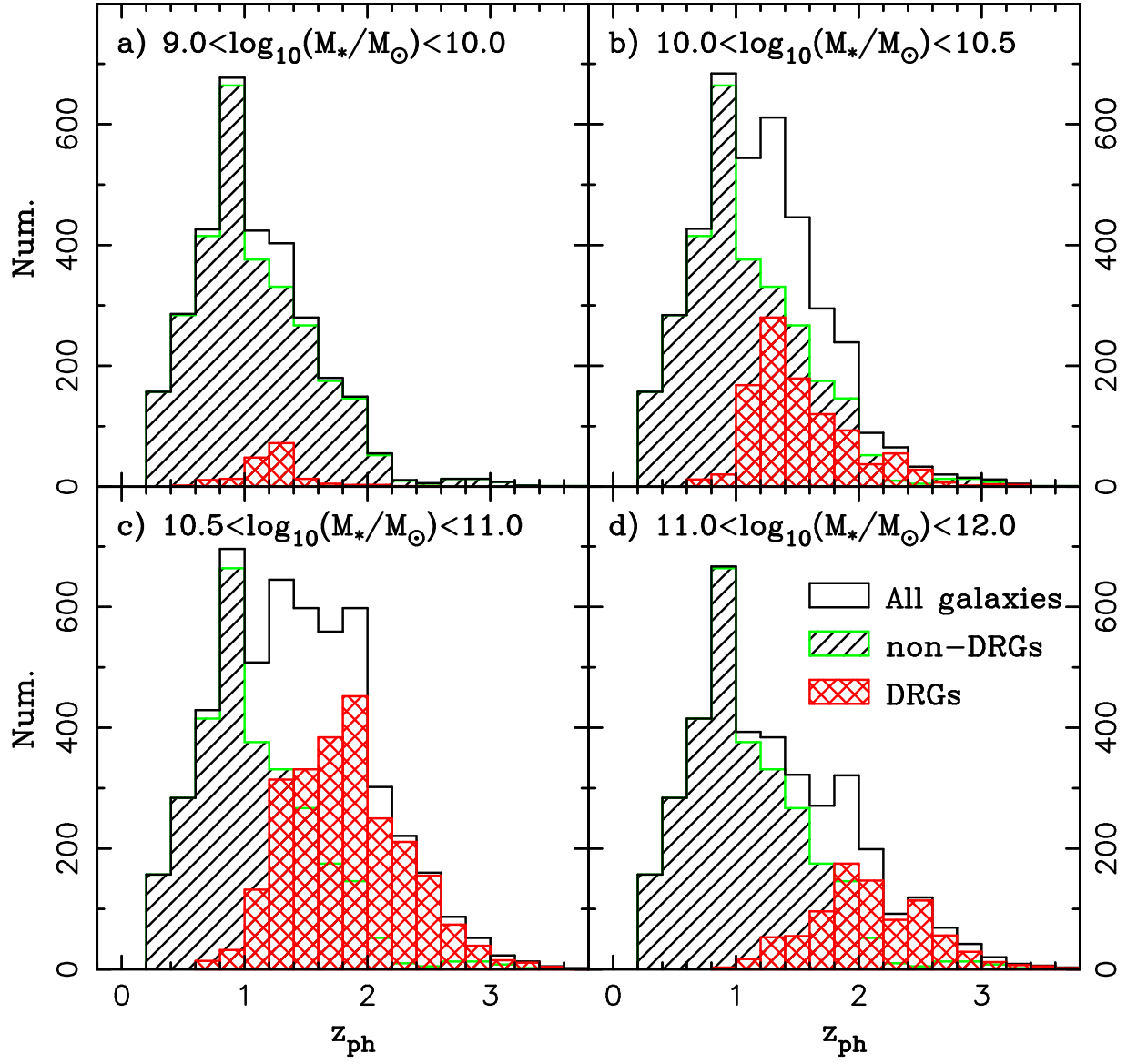


**Fig. 6.** Redshift distributions of all galaxies (black lines), DRGs (red lines) and non-DRGs (green lines) in the COSMOS/UltraVISTA field in four stellar mass bins.

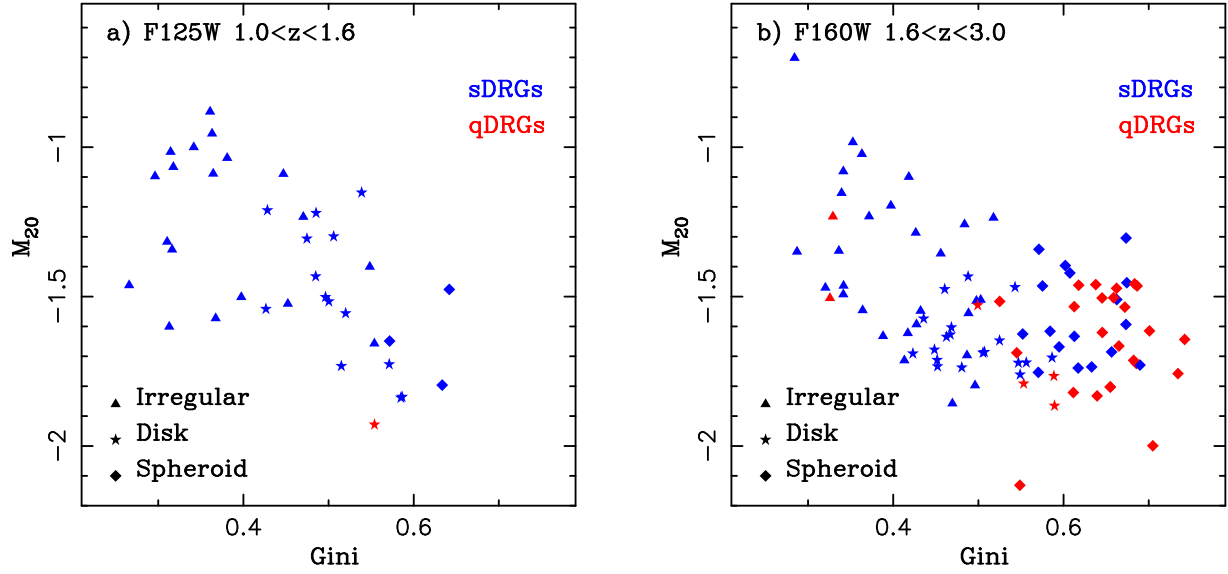


**Fig. 7.**  $M_{20}$  vs. Gini coefficient for DRGs. The star-forming DRGs (sDRGs) are plotted in blue color, while quiescent DRGs are in red. Spheroid, disk and irregular DRGs which are classified by visual inspection, are plotted in diamond, star and triangle symbols, respectively. DRGs on left panel with redshift  $1 < z < 1.6$ , whose morphological parameters are measured from F125W image. DRGs on right panel distribute at  $1.6 < z < 3$ , whose morphological parameters are measured from F160W image.

the high-mass end of the galaxy population at  $z \sim 2 - 3$ .

We have checked the mass completeness for our DRG sample, and find nearly all DRGs are above  $10^{10} M_{\odot}$  and the majority of them are above  $10^{10.5} M_{\odot}$  at  $1 < z < 3$ . The distance between the majority of DRGs and the 90% completeness boundary at  $1 < z < 3$  are safe enough, which ensures our DRG is a complete sample. Only a very small proportion of DRGs are close to the completeness boundary, and most of them are located in low-mass and low- $z$  range.

#### 4.2. Nonparametric morphology

To further describe the morphologies of these sources, we have performed nonparametric measures of galaxy morphology, such as Gini coefficient (the relative distribution of the galaxy pixel flux values, or Gini) and  $M_{20}$  (the second-order moment of the brightest 20% of the galaxy's flux) (Lotz et al. 2006), using the Morpheus-software developed by Bob Abraham (Abraham et al. 2003). Figure 7 shows the distribution of DRGs on the Gini– $M_{20}$  plane in F125W and F160W bands, which corresponds to the redshift range  $1 < z < 1.6$  and  $1.6 < z < 3$ , respectively. Diamonds, stars and triangles represent spheroid, disk and irregular galaxies, classified by visual inspection. Star-forming and quiescent DRGs classified by the rest-frame UVJ colors are plotted in blue and red, respectively. We find that most of quiescent DRGs are visually compact, and have larger Gini and smaller  $M_{20}$  values, while the star-forming DRGs contain different kinds of morphological types but most of them are visually extended and have smaller Gini and larger  $M_{20}$  values. Similar results are also reported in Lee et al. 2013 and Bassett et al. 2013.

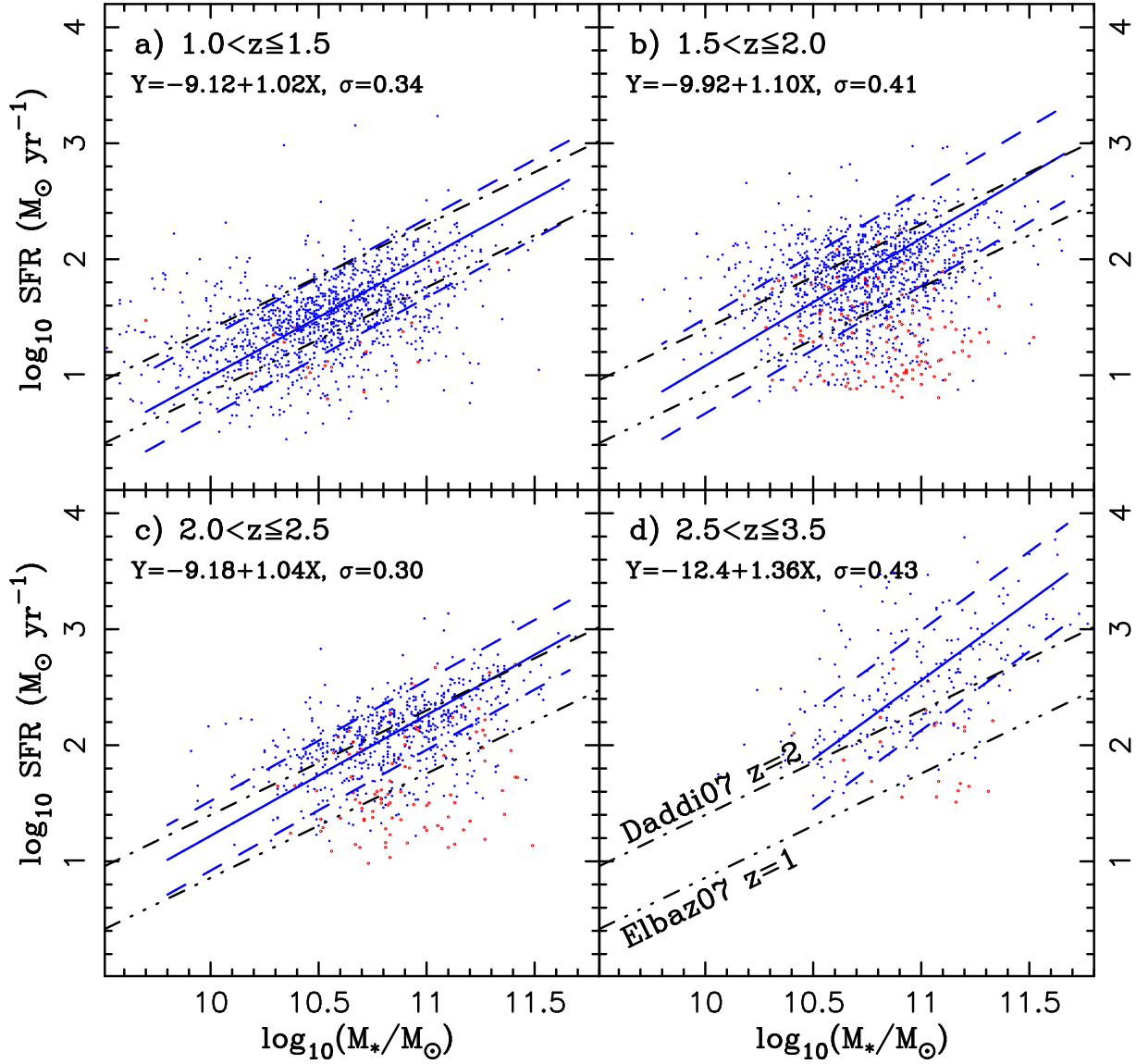
Kriek et al. 2009a; Kriek et al. 2009b support our morphological results that quiescent galaxies are commonly found to be ultra-compact, while galaxies with high SFRs have irregular and clumpy morphologies. Our morphological results also support the evolutionary tracks described in Barro et al. 2013, Bedregal et al. 2013 and Tadaki et al. 2014 that compact DRGs (with larger Gini and smaller  $M_{20}$ ) contain compact quiescent galaxies (cQGs) and their progenitors compact star-forming galaxies (cSFGs). In our sample, there are 54.5% (24/44) spheroidal DRGs are quenched, namely they are cQGs, and the rest of them are cSFGs. The cSFGs are formed by gas-rich processes such as major mergers at high redshifts, and rapidly quenched (probably by AGN) into cQGs, most of which are classified as spheroidal quiescent DRGs. These compact QGs at  $z \sim 2$  may be the cores of today’s massive elliptical galaxies, as described by van de Sande et al. 2013 and Patel et al. 2013, these quiescent galaxies at  $z \sim 2$  grow inside-out, consistent with the expectations from minor mergers.

#### 4.3. Main sequence

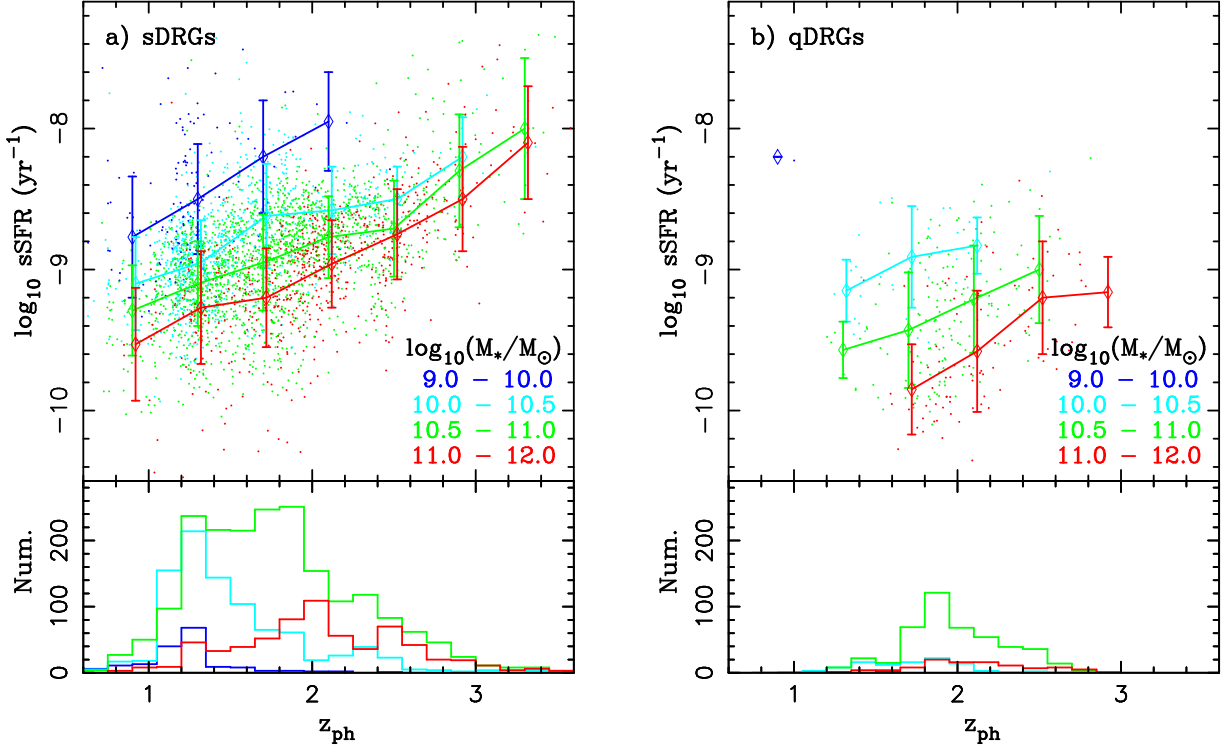
Recent studies have shown that there exists a correlation between star formation rate and stellar mass of galaxies at different redshifts ( $0 < z < 2$ ), and it is usually called “main sequence” (Brinchmann et al. 2004; Daddi et al. 2007; Elbaz et al. 2007; Pannella et al. 2009; Rodighiero et al. 2011; Barro et al. 2013; Speagle et al. 2014; Whitaker et al. 2014). To investigate the essential star formation status of DRGs, we show the “main sequence” relation in the four redshift bins in Figure 8. In this figure, the blue and red points represent star-forming and quiescent DRGs, classified by the rest-frame UVJ colors, respectively. To specify the dependence of SFR on stellar mass, we also plot a linear-fit line (blue solid line) and its  $1\sigma$  dispersion (blue dashed line) for star-forming DRGs in each redshift panel. For comparison, we overplot the best-fit “main sequence” relation for  $z \sim 2$  galaxies from Daddi et al. 2007 and  $z \sim 1$  galaxies from Elbaz et al. 2007. From this figure, we find a positive correlation between SFR and  $M_*$  of DRGs in all four redshift bins. The slopes of the SFR– $M_*$  correlation of star-forming DRGs in different redshift panels are similar. At fixed stellar masses, the SFRs of galaxies on the SFR– $M_*$  correlation increase with redshifts, which indicates that star-forming DRGs were much more active on average in the past, due to greater abundance of gas in early universe.

Figure 9 shows the dependence of specific SFR (sSFR,  $sSFR = SFR/M_*$ ) on redshifts in four  $M_*$  bins. The  $sSFR - z_{\text{ph}}$  relation of star-forming and quiescent DRGs are shown in the left and right panel, respectively. In each panel, we divide DRGs into four  $M_*$  bins (see **Figure 9**). For each  $M_*$  bin, we calculate the  $\langle sSFR \rangle$  (diamond symbols) and its standard deviation (error bars) in each redshift bin ( $\Delta z_{\text{ph}} = 0.4$ ). We find the sSFRs of DRGs increase with redshifts in all stellar mass bins, and DRGs with higher stellar masses generally have lower sSFRs. This is most likely due to the fact that the universe at early time is more active, and massive galaxies formed most of their stars earlier and slowed down more rapidly than their low-mass counterparts, star formation contributes more to the growth of low-mass galaxies





**Fig. 8.** SFR vs.  $M_*$  diagram for DRGs in four redshift bins. Star-forming DRGs are plotted in blue points, quiescent DRGs are plotted in red points. The blue lines represent the best-fit of the main sequence of star-forming DRGs, and the blue dashed lines represent the  $1\sigma$  dispersion. For comparison, the best-fit lines from Daddi et al. 2007 and Elbaz et al. 2007 are also plotted.



**Fig. 9.** sSFR vs.  $z_{\text{ph}}$  diagram for star-forming DRGs in left panel and quiescent DRGs in right panel. DRGs in different mass bins are plotted with different colors. The diamond symbols represent average sSFR value in redshift bin  $\Delta z_{\text{ph}} = 0.4$ , and the error bars represent its  $1\sigma$  deviation. The histograms in the bottom panels show the redshift distributions of DRGs.

than high-mass galaxies. This result is in agreement with the “downsizing” mass-dependent quenching scenario (Kajisawa et al. 2010; Kajisawa et al. 2011).

#### 4.4. Star forming status and $[3.6]-[24]$ color

The total SFR of galaxy we used are determined via  $\text{SFR}_{\text{tot}} = \text{SFR}_{\text{UV,uncorr}} + \text{SFR}_{\text{IR}}$  (Muzzin et al. 2013a). The  $\text{SFR}_{\text{UV,uncorr}}$  comes from SED fitting method and the  $\text{SFR}_{\text{IR}}$  is derived by  $24 \mu\text{m}$  flux. Higher fraction of  $\text{SFR}_{\text{IR}}$  in  $\text{SFR}_{\text{tot}}$  means there are more UV photons absorbed by dust, and these energies are re-emitted from IR range. We plot the  $\text{SFR}_{\text{IR}}/\text{SFR}_{\text{tot}}$  vs.  $M_*$  of all galaxies (left panel) and DRGs (right panel, red points for qDRGs, and blue points for sDRGs) in Figure 10. From this figure we find there exists a trend in the  $\text{SFR}_{\text{IR}}/\text{SFR}_{\text{tot}}$  vs.  $M_*$  diagram of all galaxies: high-mass galaxies tend to have higher  $\text{SFR}_{\text{IR}}/\text{SFR}_{\text{tot}}$  ratios, indicating that massive galaxies tend to contain more dust and they are more metal rich, thus the extinction for UV lights are heavier than low-mass galaxies. Similar results are also found by Tadaki et al. 2013 in their H $\alpha$  emitter (HAE) sample. We also find DRGs occupy the high-mass and high ratio of  $\text{SFR}_{\text{IR}}/\text{SFR}_{\text{tot}}$  region, which suggests the  $J-K$  color criterion effectively selects the massive dusty sources whose  $\text{SFR}_{\text{IR}}$  are dominant. As the  $\text{SFR}_{\text{IR}}/\text{SFR}_{\text{tot}}$  of most of DRGs great than 95%, it is suitable for DRGs using the  $24 \mu\text{m}$  derived  $\text{SFR}_{\text{IR}}$  to trace the whole star formation activity.

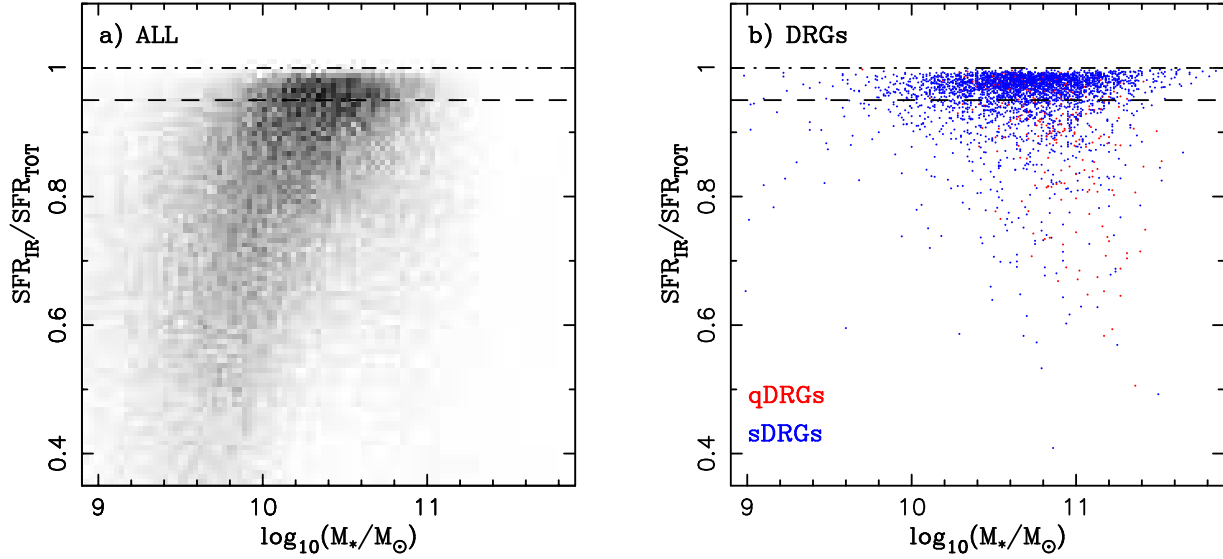


**Fig. 10.**  $\text{SFR}_{\text{IR}}/\text{SFR}_{\text{tot}}$  vs. stellar mass ( $M_*$ ) diagram for DRGs (right panel) and all galaxies in the COSMOS/UltraVISTA field (left panel). The dashed line corresponds to  $\text{SFR}_{\text{IR}}/\text{SFR}_{\text{tot}} = 95\%$ .

There are 29.4% quiescent and 49.8% star-forming all  $K$ -selected galaxies in our sample have both [3.6] and [24] detection, and there are 37.3% quiescent and 87.7% star-forming DRGs have been detected at [3.6] and [24] bands simultaneously. The origins of the  $24\mu\text{m}$  fluxes of the quiescent population can be due to processes unrelated to ongoing star formation, such as AGNs, cirrus dust heated by old stellar populations and circumstellar dust. Fumagalli et al. 2014 treat each of these components separately and compare their contributions to  $L_{\text{IR}}$  with the observed stacked values of  $L_{\text{IR}}$ , and conclude that various processes other than star formation can contribute to the observed mid-IR flux, thus the  $24\mu\text{m}$ -derived SFRs for quiescent galaxies should be the upper limits.

At the redshift  $z \sim 1 - 3$ , the IRAC 3.6  $\mu\text{m}$  probes the rest-frame NIR range, which can be derived into stellar mass (Bell & de Jong 2001; Cole et al. 2001). The left panel of Figure 11 shows the relationship of [3.6] vs.  $M_*$  of all DRGs. We divide DRGs into four redshift bins, and find there exists a strong correlation between [3.6] and  $M_*$ . The linear-fit standard deviations of four redshift bins (from low to high) are 0.25, 0.20, 0.12 and 0.16, respectively. Similarly, the strong correlation between sSFRs and [3.6]–[24] colors in wide redshift range ( $1 < z < 3.5$ ) are also found in the right panel of Figure 11. The standard deviations of linear fit of four redshift bins (from low to high) are 0.21, 0.19, 0.17 and 0.27, respectively. The average [3.6]–[24] color of quiescent all  $K$ -selected galaxies is 0.78, while star-forming all  $K$ -selected galaxies is 2.03. For our DRG sample, the average [3.6]–[24] color of quiescent DRG is 1.57, while star-forming DRG is 2.25. The [3.6]–[24] color of most of these  $24\mu\text{m}$ -detected quiescent DRGs are generally consistent with but slightly redder than that of QGs presented by Brammer et al. 2009, Wang et al. 2012 and Huang et al. 2013, who identify QGs with the empirical [3.6]–[24] color criterion which is equivalent to a  $\text{sSFR} \sim 10^{-10}(\text{yr}^{-1})$ . Quiescent and star-forming populations separate

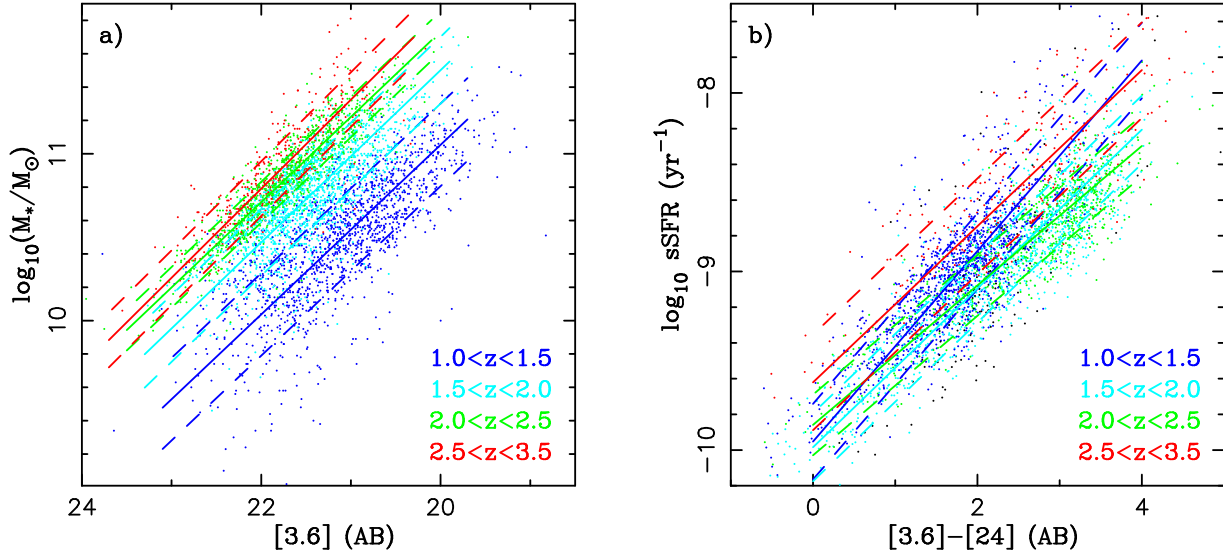


**Fig. 11.** Left panel: correlation between stellar mass and 3.6  $\mu\text{m}$  magnitude of DRGs. Right panel: correlation between sSFR and [3.6]–[24] color of DRGs. DRGs in different redshift bins are plotted in different colors. Solid lines are best-fit lines for each redshift bin, dashed lines represent  $1\sigma$  deviation.

obviously in both DRG and all  $K$ -selected galaxy samples, which implies that [3.6]–[24] color is a good indicator for tracing star-forming status of galaxies. The similar results were also described in Huang et al. 2013.

To demonstrate how the DRG selection picks up each type of galaxies, we show the fraction of quiescent galaxies and the fraction of dusty star-forming galaxies with  $\text{SFR}_{\text{IR}}/\text{SFR}_{\text{tot}} > 0.95$  selected by the DRG criterion as a function of redshift in Figure 12. Based on the stellar mass distribution of DRGs, we show the fractions for QGs and SFGs in three mass bins:  $10 < \log_{10}(M_*/M_\odot) < 10.5$ ,  $10.5 < \log_{10}(M_*/M_\odot) < 11$  and  $11 < \log_{10}(M_*/M_\odot) < 12$ , which are represented by the three columns of Figure 12 from left to right. The panels in the top and bottom row are fractions for QGs and SFGs, respectively. From this figure we find that (1) Higher fraction of dusty SFGs with  $\text{SFR}_{\text{IR}}/\text{SFR}_{\text{tot}} > 0.95$  will be selected as DRG in higher mass bins, while the fractions of QGs remain nearly constant from low to high mass ranges; (2) Both fractions of QGs and SFGs increase with redshift in each stellar mass bin, but the increase for QGs are more dramatic: very few QGs can be selected as DRG at  $z < 2$ , while at  $z > 2$  the fraction suddenly rises to a very high level. The result shown by this figure indicates that heavy dust reddening of  $J - K$  color exists among high-mass SFGs, while the  $J - K$  color of QGs is irrelevant to mass, because there is no dust extinction, the dramatic increase of the fraction of QGs is due to the sharp Balmer or 4000  $\text{\AA}$  breaks of older stellar population shift into  $J$ -band at  $z > 2$ .

#### 4.5. Rest frame $U-V$ color vs. stellar mass

Galaxies present bi-modal distribution on the rest-frame color vs. mass diagram (CMD), and they show red rest-frame colors due to dust extinction or old stellar ages, thus the bi-

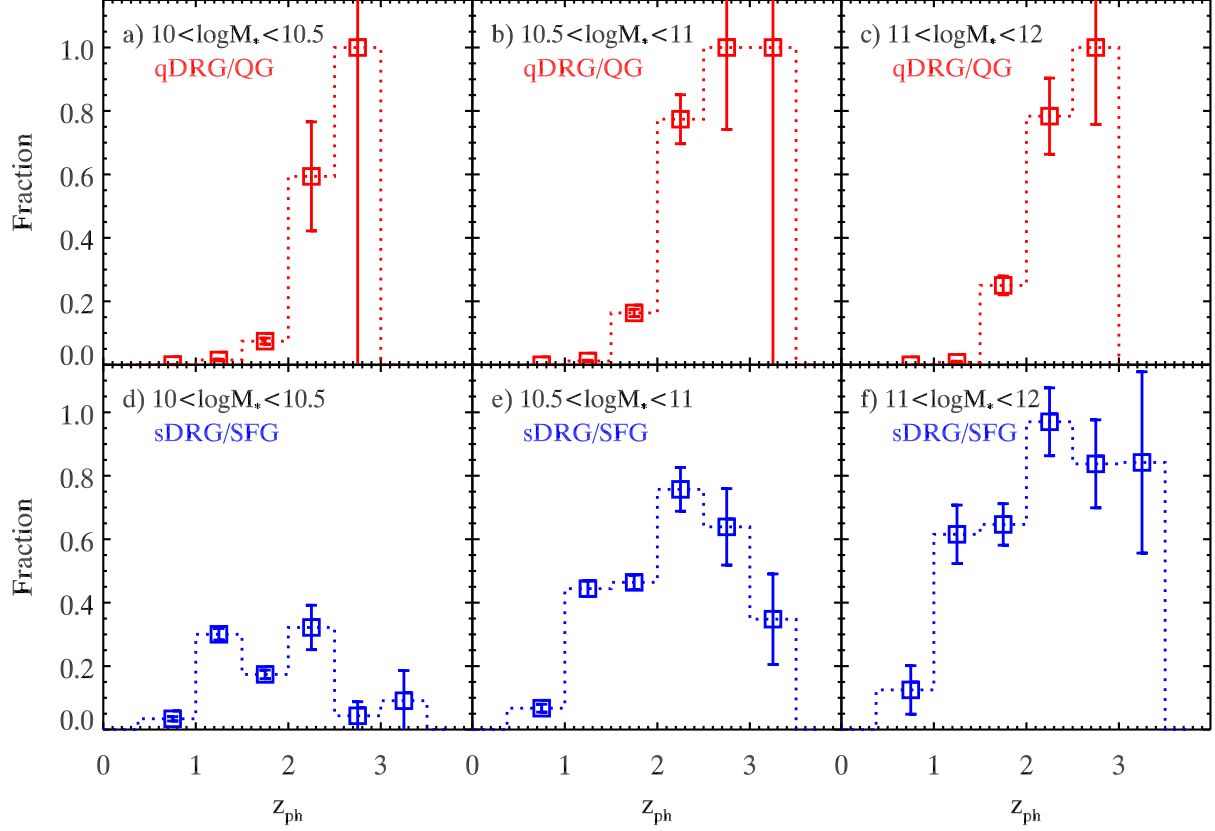


**Fig. 12.** Panel a), b) and c): Fraction of quiescent galaxies selected by the DRG criterion as a function of redshift. Panel d), e) and f): Fraction of dusty star-forming galaxies with  $\text{SFR}_{\text{IR}}/\text{SFR}_{\text{tot}} > 0.95$  selected by the DRG criterion as a function of redshift. The fractions of QGs and SFGs are shown in three stellar mass bins ( $\log_{10}(M_*/M_\odot)=10-10.5$ ,  $10.5-11$  and  $11-12$ ), and in each mass bin we divide them into six redshift bins ( $z=0.5-1$ ,  $1-1.5$ ,  $1.5-2$ ,  $2-2.5$ ,  $2.5-3$  and  $3-3.5$ ) to calculate the fractions.

modal distribution on CMD suggests two distinct types of galaxy formation histories (Bell et al. 2004; Cassata et al. 2008; Brammer et al. 2009). Talia et al. 2013 shows the good correlation between  $(U - B)_{\text{rest}}$  and stellar mass, galaxies with redder  $(U - B)_{\text{rest}}$  colors are more massive, no matter what kind of morphologies they are. Wang et al. 2012 find that disk galaxies tend to be more massive and have redder  $(U - V)_{\text{rest}}$  colors than irregular galaxies in their IERO sample. Díaz Tello et al. 2013 showed that with a particular  $(u - B)$  color, the high-redshift galaxies had on average higher sSFRs.

Figure 13 shows the distribution of DRGs on  $(U - V)_{\text{rest}}$  vs.  $M_*$  diagram in six redshift bins. Star-forming and quiescent DRGs are plotted in blue and red, respectively. DRGs having visual morphological types introduced in Section 3.3 are also plotted in corresponding symbols. We find that the  $(U - V)_{\text{rest}}$  color and  $M_*$  of DRGs correlate very well in all redshift bins, which is in good agreement with Figure 10: more massive galaxies have redder  $(U - V)_{\text{rest}}$  colors due to their larger internal dust extinctions or old stellar ages, which is also presented by Kajisawa & Yamada 2006. However, star-forming and quiescent DRGs cannot be separated efficiently

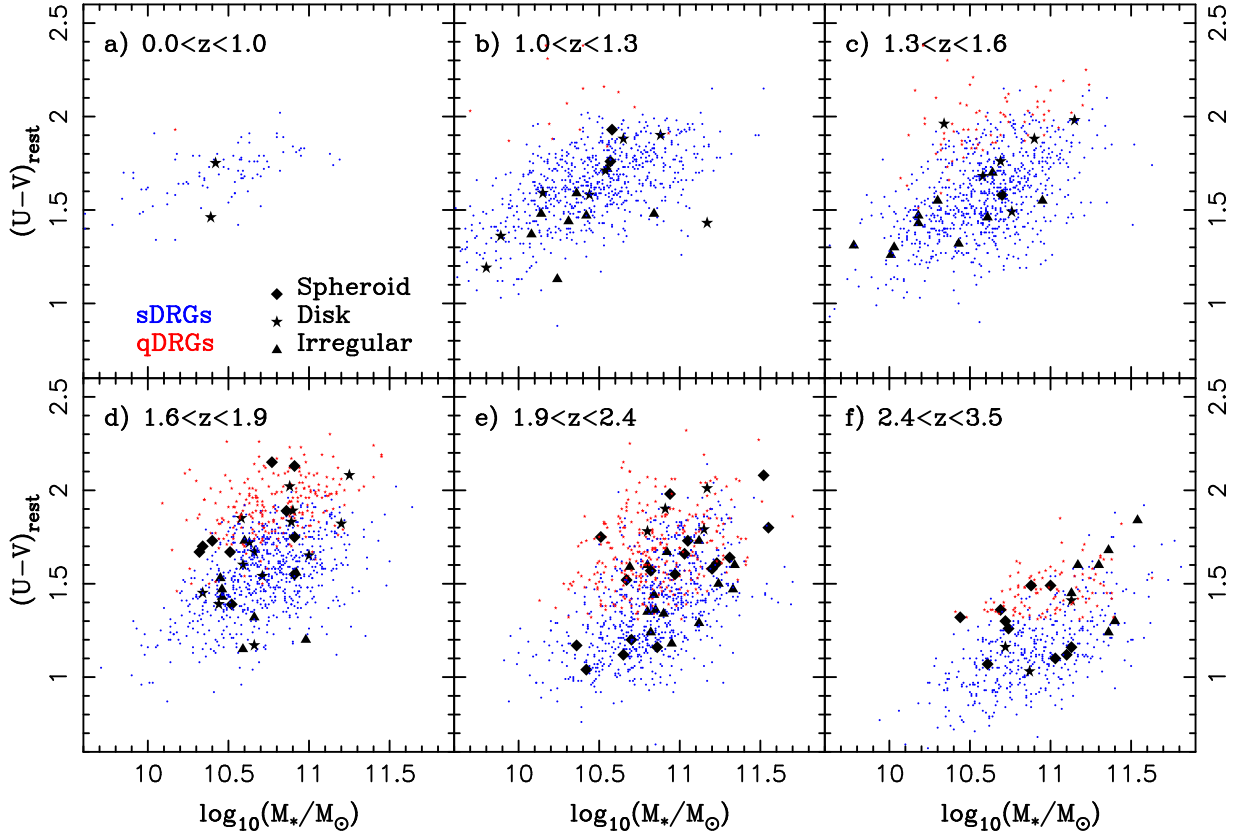


**Fig. 13.** Rest-frame  $(U - V)_{\text{rest}}$  color vs. stellar mass diagram for DRGs in six redshift bins. Star-forming DRGs and quiescent DRGs are plotted in blue and red points, respectively. DRGs which have visual morphological types are also plotted in corresponding symbols.

on CMD, they do not present clear bimodality, which is similar to what Wang et al. 2012 and Huang et al. 2013 have found. DRGs with similar stellar masses have bluer  $(U - V)_{\text{rest}}$  colors at high redshifts, implying DRGs evolve with time, they gradually consume matter materials and eventually slow down their star forming activities (Kajisawa & Yamada 2005). We also find that the irregular DRGs dominate the reddest  $(U - V)_{\text{rest}}$  color and high-mass end at high-redshifts, but gradually turn bluer and less massive than disk and spheroid DRGs toward low-redshifts. At  $z > 1.6$ , there are many blue spheroid DRGs, they are in the stage of compact star-forming galaxies, which are supposed to be the progenitors of compact QGs at high redshift. The findings above may indicate a possible evolution scenario that massive disk-like DRGs merge with each other frequently by dissipative major merger at high redshifts, and produce massive dust-obscured irregular star-bursts, then through violent relaxation and angular momentum loss, they become spheroid-like DRGs and then quenched at later epoch. The findings are also supported by Bedregal et al. 2013, Barro et al. 2013, Bassett et al. 2013 and Williams et al. 2014.



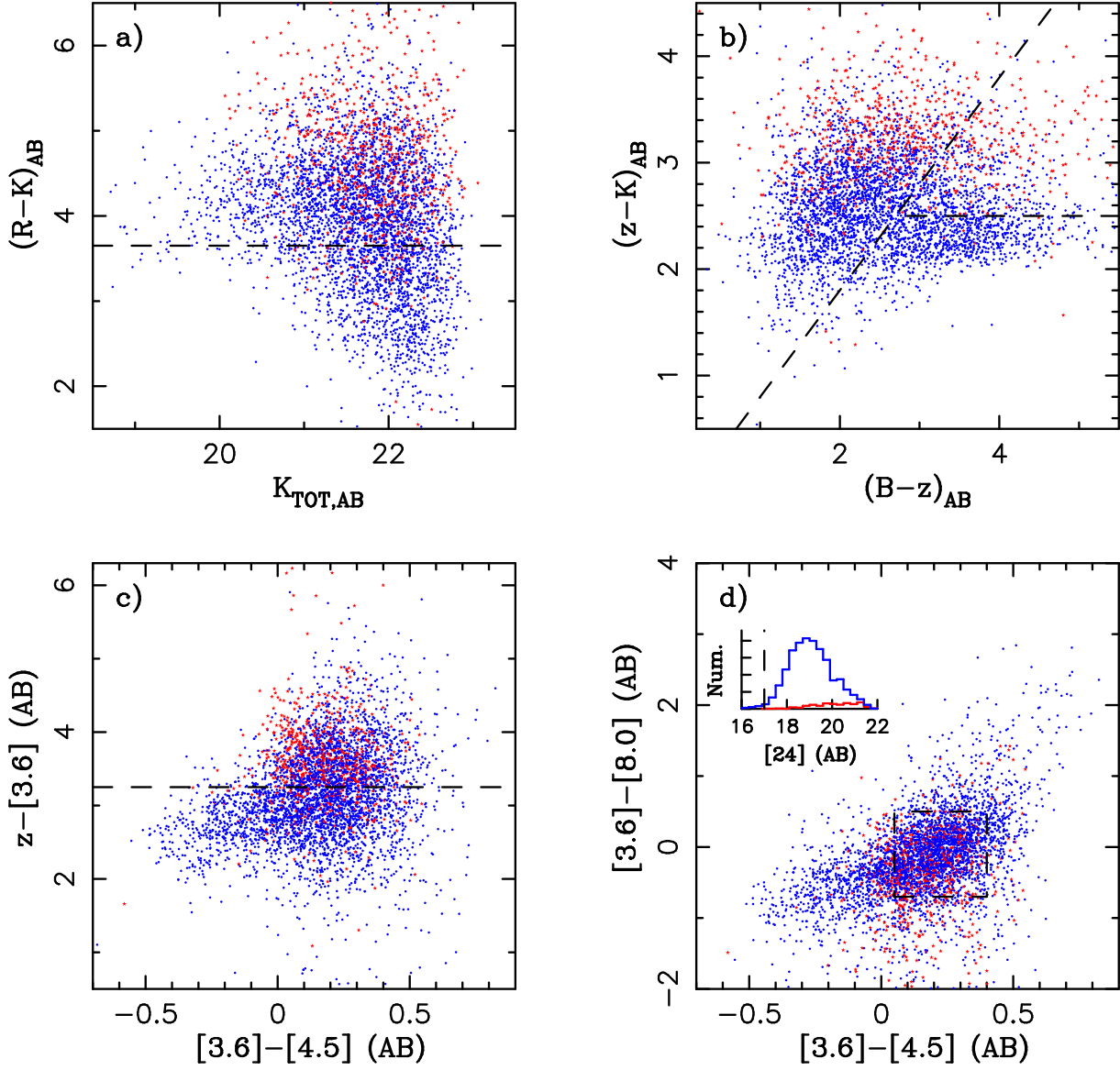


**Fig. 14.** (a): Distribution of star-forming DRGs (blue) and quiescent DRGs (red) on ERO selection diagram. The selection criteria are introduced in Simpson et al. 2006 and Lane et al. 2007. (b): Distribution of DRGs on BzK selection diagram. The selection criteria are defined by Daddi et al. 2004. (c): Distribution of DRGs on IERO selection diagram. The selection criteria are defined by Yan et al. 2004. (d): Distribution of DRGs on high- $z$  ULIRG selection diagram. This selection criteria are defined by Huang et al. 2009. The insert panel show the distribution of DRGs on the Spitzer 24  $\mu m$  magnitude.

## 5. Compare DRG to other color-selected high-redshift galaxies

Over the past decade, many color selection techniques, which are designed based on rest-frame spectral energy distribution features, are applied to identify high-redshift galaxies (Steidel et al. 1996; Smail et al. 1997; Franx et al. 2003; Daddi et al. 2004; Gronwall et al. 2007; Yan et al. 2007; Dey et al. 2008; Dunne et al. 2009; Huang et al. 2009; Caputi et al. 2012; Wang et al. 2012; Arcila-Osejo & Sawicki 2013; Ilbert et al. 2013). However, due to the small sizes of samples used in previous works, the overlaps between DRG and other color selected population have not been well studied. In this section, we use our large DRG sample to study the overlaps between DRGs and EROs, BzKs, IEROs and high redshift ULIRGs.

First of all, we study the overlap between DRGs and EROs. To be consistent with Kong et al. 2006 and Lane et al. 2007, we use  $R-K$  color to select EROs from DRG sample. The color criterion  $(R_{\text{Subaru}} - K_{\text{UKIDSS}})_{\text{vega}} > 5.3$  in Lane et al. 2007 can be converted to  $(R-K)_{\text{AB}} > 3.65$  via  $R_{\text{AB}} = R_{\text{vega}} + 0.22$  and  $K_{\text{AB}} = K_{\text{vega}} + 1.87$ . Figure 14 (a) shows the distribution of DRGs onto  $(R-K)$  vs.  $K$  diagram. We find that the distribution on  $K$  of quiescent DRGs is similar to star-forming DRGs. However, the distributions of quiescent and star-forming DRGs on  $R-K$  color are obviously different, quiescent DRGs have much redder  $R-K$  colors than star-forming DRGs, which attributes to the SED features of old stellar populations in quiescent DRGs. 69% DRGs can be selected as ERO, which represents the low redshift range of DRG population. Many DRGs especially sDRGs distribute at higher redshift are missed by the ERO selection.

Secondly, we follow the procedure of McCracken et al. 2010 to perform  $B-z$  color calibration and correct the  $K$  band accounting for  $K_{\text{UltraVISTA}} - K_{\text{WIRCam}} = 0.051$  described in Muzzin et al. 2013a, to see how DRGs satisfy the BzK criteria. Figure 14 (b) shows the distribution of DRGs on the  $(z-K)$  vs.  $(B-z)$  plane. Star-forming DRGs are slightly bluer than quiescent DRGs on  $B-z$  color, but are obviously bluer on  $z-K$  color. 60.4% DRGs could be selected as sBzKs, 17.7% DRGs could be selected as pBzKs. Other DRGs mainly distribute in the redshift range of  $z < 1.4$ , most (73%) of which are EROs.

Thirdly, we analyze the overlap between DRGs and IEROs color criterion which is introduced by Yan et al. 2004. The purpose of IERO method is designed for selecting massive galaxies with mature stellar populations at  $z \sim 2$  based on 4000 Å Balmer break shifting beyond  $z$ -band or steep slope of the rest-frame UV spectra of galaxies. Thus, a simple color cut  $z-[3.6]$  is designed to select high redshift galaxies. Young and blue galaxies cannot reach this threshold even at higher redshifts (Wang et al. 2012). Based on the simulation performed by continuous star formation (CSF) models in BC03 code, we obtain  $z_{\text{ACS}} - z_{\text{Subaru}} = -0.11$  to calibrate  $z$ -band. As shown in Figure 14 (c), distributions on  $[3.6]-[4.5]$  color of two population of DRGs are almost the same. However, star-forming DRGs are obviously bluer than quiescent DRGs on  $z-[3.6]$  color. There are 72% quiescent DRGs and 39% star-forming DRGs could be selected as IERO. Quiescent DRGs are more likely to be selected as IERO, the IERO color criterion rules

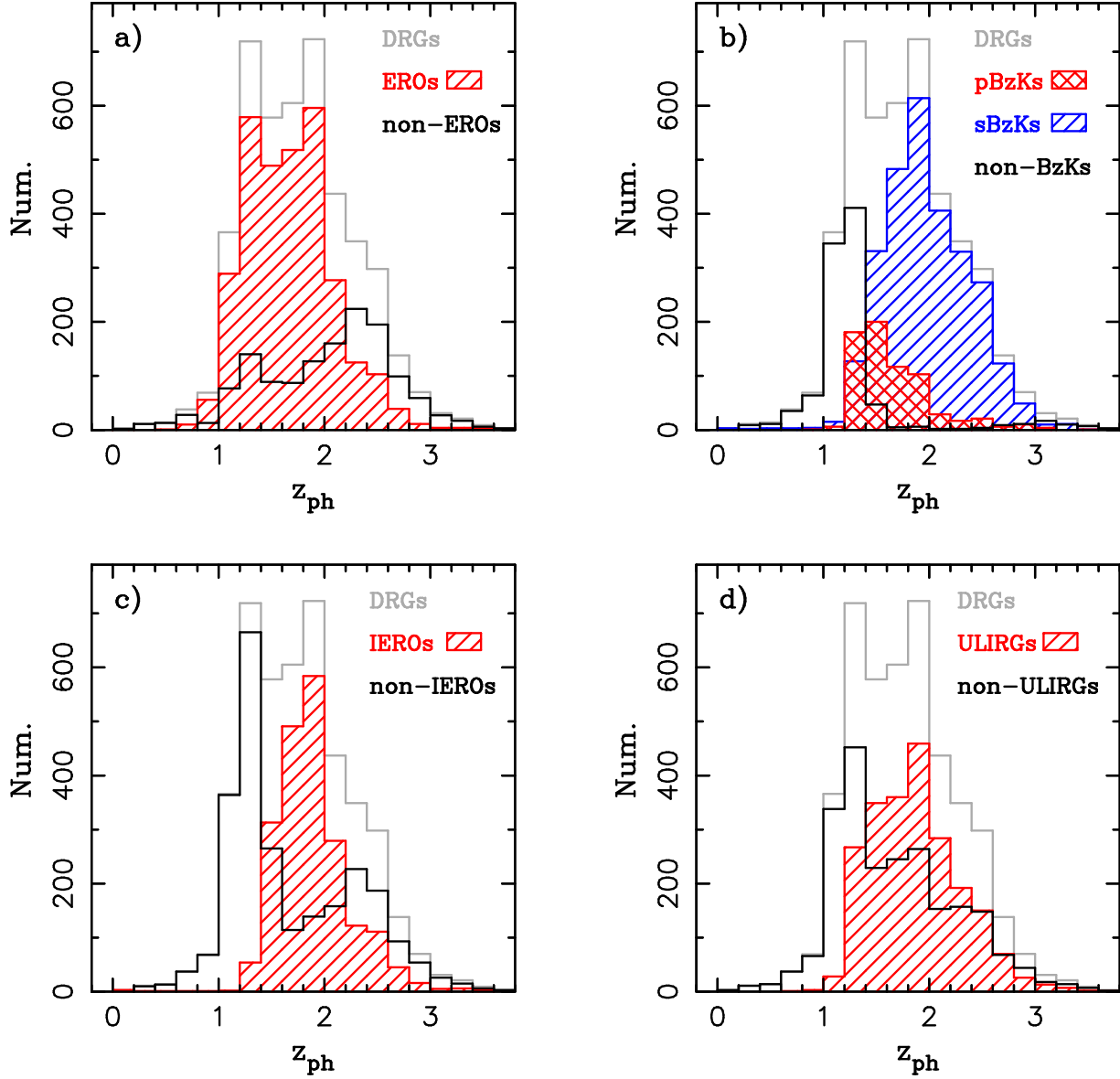


**Fig. 15.** Redshift distributions of DRGs that satisfy the ERO, BzK, IERO and high- $z$  ULIRG color criteria. Red lines represent the distribution of DRGs satisfying the corresponding color criterion in each panel and black lines represent remanent DRGs.

out a large proportion of star-forming DRGs, most of which are low-mass star-forming galaxies at low redshifts.

Lastly, we perform comparison between DRG and high- $z$  ULIRG color criteria introduced by Huang et al. 2009. This IRAC color selection method is designed for selecting massive, star-forming dominated ULIRGs at  $z \sim 2$  based on the  $1.6 \mu\text{m}$  stellar emission bump feature in galaxy SEDs. In  $1.5 < z < 3$ , the four IRAC bands probe the rest-frame NIR bands where galaxy SEDs have similar shape, thus the IRAC colors are robust in determining redshift in this range (Huang et al. 2009). The color criterion is set as  $0.05 < [3.6] - [4.5] < 0.4$  and  $-0.7 < [3.6] - [8.0] < 0.5$  based on the M82 SED model (Huang et al. 2004). Figure 14 (d)

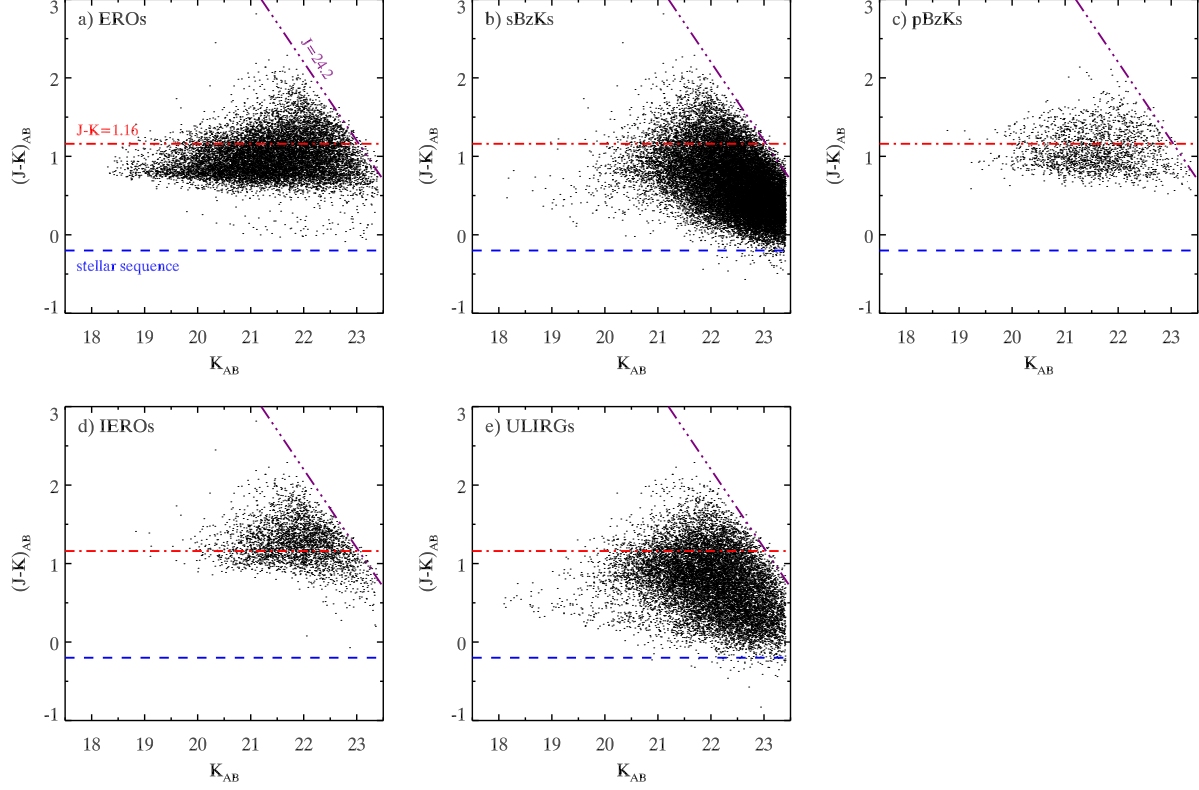


**Fig. 16.** Distributions of other color-selected galaxies on the DRG selection diagram. Panel a), b), c), d) and e) shows the distribution of ERO, sBzK, pBzK, IERO and high- $z$  ULIRG, respectively.

shows the distribution of DRGs on the  $[3.6]-[8.0]$  vs.  $[3.6]-[4.5]$  diagram. We find that the peaks of DRGs on both two colors fall into the selection region designed by Huang et al. 2009, 49.2% DRGs can be selected by this rectangle region, which reflects this selection method is efficient in determining redshifts. However, there are only 1.3% of DRGs satisfy their third cut,  $F_{24\mu\text{m}} > 0.5$  mJy, which is correspond to 17.15 mag in AB, as shown in the insert panel of Figure 14 (d). Figure 15 shows the redshift distributions of DRGs, and the subsample of DRG satisfying other color criteria. We find that a large proportion of DRGs could also be selected as ERO, they mainly distribute at  $z \sim 1$ , most of which are dust reddened star-forming galaxies. The BzK method is very sharp in determining redshifts. Most of DRGs in our sample can be selected as sBzKs or pBzKs which distribute at  $z > 1.4$ , non-BzKs mainly distribute at  $z < 1.4$ . The IERO criterion introduced by Wang et al. 2012 and the high- $z$  ULIRG criterion introduced by Huang et al. 2009 are all efficient in selecting  $z \sim 2$  galaxies.

Similarly, we show how other color-selected galaxies satisfy the DRG selection criterion in Figure 16. Panel a), b), c), d) and e) shows the distribution on the DRG selection  $J - K$  vs.  $K$  diagram for ERO, sBzK, pBzK, IERO and ULIRG, respectively. 24.3% EROs, 10.7% sBzKs, 34.4% pBzKs, 64.1% IEROs and 15.8% high- $z$  ULIRGs (not include the  $24\mu\text{m}$  flux criterion)

can be selected as DRG by the criterion  $J - K > 1.16$ . From the comparisons performed above, we can get a clear point of view in different color selection criteria: methods designed for selecting galaxies at  $z \sim 2$  have many overlaps between each other. The DRG population is not a special galaxy group, the redshift distribution of them is broad, and most of them can also be selected by other color criterion.

## 6. Summary

In this paper, we have described the construction of a large DRG sample in the COSMOS/UltraVISTA field. Based on multi-band photometry data, we analyze the physical properties of DRGs. Our main conclusions are as follows.

1. We select a sample of 4485 DRGs with  $(J - K)_{\text{AB}} > 1.16$  and  $K_{\text{AB}} < 23.4$  mag, and identify 3725 star-forming DRGs and 760 quiescent DRGs based on rest-frame UVJ colors. We find the redshift distributions of DRGs are broad, ranging from 0.5 to 3.5 with a mean value of 1.79, but most of them (95.5%) distribute at  $1 < z < 3$ . The stellar masses of DRGs mainly distribute at  $10^{10} M_{\odot} - 10^{11.5} M_{\odot}$ . DRGs represent 70% of all galaxies in higher-mass bins at  $z > 2$ , indicating that the DRG selection criterion is sensitive to select massive galaxies at high redshift.

2. We study the morphological properties of DRGs in our sample, employing data from *HST* WFC3/F125W and F160W imaging within the COSMOS field. For DRGs distribute at  $1 < z < 1.6$  and  $1.6 < z < 3$ , we measure Gini and  $M_{20}$  from F125W and F160W images, respectively. The morphological results are consistent with our rest-frame UVJ color classification: quiescent DRGs are generally compact and star-forming DRGs tend to have extended structures, implying that these galaxies have experienced different formation processes.

3. The SFR and  $M_*$  of star-forming DRGs present good “main sequence” relations in all redshift bins. Moreover, the sSFR of DRGs increase with redshift in all stellar mass bins and DRGs with higher stellar masses generally have lower sSFRs, which indicates that galaxies were much more active on average in the past, and star formation contributes more to the mass growth of low-mass galaxies than to high-mass galaxies, owing to massive galaxies formed most of their stars earlier and rapidly slow down than their low-mass counterparts. This result is in agreement with the “downsizing” scenario.

4. There exists a trend in the  $\text{SFR}_{\text{IR}}/\text{SFR}_{\text{tot}}$  vs.  $M_*$  diagram of all galaxies: high-mass galaxies tend to have higher  $\text{SFR}_{\text{IR}}/\text{SFR}_{\text{tot}}$  ratios, indicating that massive galaxies tend to contain more dust, thus the extinction for UV lights are heavier than low-mass galaxies. We find DRGs occupy the high-mass and high ratio of  $\text{SFR}_{\text{IR}}/\text{SFR}_{\text{tot}}$  region, which suggests the  $J - K$  color criterion effectively selects the massive dusty sources whose  $\text{SFR}_{\text{IR}}$  are dominant, and it is suitable for DRGs using  $[3.6] - [24]$  color to trace their sSFRs. The fraction of QGs and the fraction of SFGs with  $\text{SFR}_{\text{IR}}/\text{SFR}_{\text{tot}} > 0.95$  selected by DRG criterion as a function of redshift indicate that the red  $J - K$  colors are mainly caused by dust reddening for SFGs and

the Balmer or 4000 Å breaks shifting into the  $J$ -band at  $z > 2$  for QGs.

5. The  $(U - V)_{\text{rest}}$  color strongly correlates  $M_*$  of DRGs in all redshift bins. Massive DRGs have redder  $(U - V)_{\text{rest}}$  colors and the  $(U - V)_{\text{rest}}$  colors of DRGs become bluer at higher redshifts, suggesting high-mass galaxies have larger internal dust extinctions or older stellar ages and they evolve with time. We also find that the irregular DRGs dominate the reddest  $(U - V)_{\text{rest}}$  color and high-mass end at high-redshifts, but gradually turn bluer and less massive than disk and spheroid DRGs toward low-redshifts. At  $z > 1.6$ , there are many blue spheroid DRGs. They are in the stage of compact star-forming galaxies which are supposed to be the progenitors of compact QGs at high redshift. These findings may indicate a possible evolution scenario that massive disk-like DRGs merge with each other frequently, then through violent relaxation and angular momentum loss, they finally become spheroid-like galaxies.

6. We study the overlaps between DRGs and EROs, BzKs, IEROs, high- $z$  ULIRGs, find DRGs in our sample can be selected by other color criteria also. 69% DRGs can be selected as EROs, and most of them have low redshift. 60% DRGs can be selected as sBzKs, 18% DRGs can be selected as pBzKs, non-BzKs mainly distribute at  $z < 1.4$ , most (73%) of them are EROs. 72% quiescent DRGs and 39% star-forming DRGs could be selected as IERO, quiescent DRGs are more likely to be selected as IERO, the IERO color criterion rules out a large proportion of star-forming DRGs, most of them are low-mass star-forming galaxies at low redshifts. 49% DRGs can be selected by the rectangle region of high- $z$  ULIRG candidates and only 1.3% of DRGs in our sample satisfy the  $F_{24\mu\text{m}} > 0.5\text{mJy}$  flux cut, which introduced by Huang et al. 2009. In turn, 24.3% EROs, 10.7% sBzKs, 34.4% pBzKs, 64.1% IEROs and 15.8% high- $z$  ULIRGs (not include the  $24\mu\text{m}$  flux criterion) can be selected as DRG by the criterion  $J - K > 1.16$ .

## Acknowledgments

We are grateful to R. Abraham for access to his morphology analysis code. We also acknowledge E. Daddi and A. Muzzin for their valuable comments. This work is based on observations taken by the CANDELS Multi-Cycle Treasury Program with the NASA/ESA HST, which is operated by the Association of Universities for Research in Astronomy, Inc., under the NASA contract NAS5-26555. This work is supported by the National Natural Science Foundation of China (NSFC, Nos. 11303002, 11225315, 1320101002, 11433005, and 11421303), the Specialized Research Fund for the Doctoral Program of Higher Education (SRFDP, No. 20123402110037), the Strategic Priority Research Program “The Emergence of Cosmological Structures” of the Chinese Academy of Sciences (No. XDB09000000), the Chinese National 973 Fundamental Science Programs (973 program) (2015CB857004), the Yunnan Applied Basic Research Projects (2014FB155) and the Open Research Program of Key Laboratory for Research in Galaxies and Cosmology, CAS.



## References

- Abraham, R. G., van den Bergh, S., & Nair, P. 2003, *ApJ*, 588, 218
- Arcila-Osejo, L., & Sawicki, M. 2013, *MNRAS*, 435, 845
- Barro, G., Pérez-González, P. G., Gallego, J., et al. 2011, *ApJS*, 193, 30
- Barro, G., Faber, S. M., Perez-Gonzalez, P. G., et al. 2013, *ApJ*, 765, 104
- Bassett, R., Papovich, C., Lotz, J. M., et al. 2013, *ApJ*, 770, 58
- Bedregal, A. G., Scarlata, C., Henry, A. L., et al. 2013, *ApJ*, 778, 126
- Bell, E. F., & de Jong, R. S. 2001, *ApJ*, 550, 212
- Bell, E. F., Wolf, C., Meisenheimer, K., et al. 2004, *ApJ*, 608, 752
- Brammer, G. B., van Dokkum, P. G., & Coppi, P. 2008, *ApJ*, 686, 1503
- Brammer, G. B., Whitaker, K. E., van Dokkum, P. G., et al. 2009, *ApJL*, 706, L173
- Brinchmann, J., Charlot, S., White, S. D. M., et al. 2004, *MNRAS*, 351, 1151
- Bruzual, G., & Charlot, S. 2003, *MNRAS*, 344, 1000
- Capak, P., Aussel, H., Ajiki, M., et al. 2007, *ApJS*, 172, 99
- Caputi, K. I., Dunlop, J. S., McLure, R. J., et al. 2012, *ApJL*, 750, L20
- Cassata, P., Cimatti, A., Kurk, J., et al. 2008, *A&A*, 483, L39
- Chapman, S. C., Blain, A. W., Ivison, R. J., & Smail, I. R. 2003, *Nature*, 422, 695
- Chary, R., & Elbaz, D. 2001, *ApJ*, 556, 562
- Cole, S., Norberg, P., Baugh, C. M., et al. 2001, *MNRAS*, 326, 255
- Conselice, C. J., Newman, J. A., Georgakakis, A., et al. 2007, *ApJL*, 660, L55
- Cowie, L. L., Songaila, A., Hu, E. M., & Cohen, J. G. 1996, *AJ*, 112, 839
- Daddi, E., Cimatti, A., Renzini, A., et al. 2004, *ApJ*, 617, 746
- Daddi, E., Dickinson, M., Chary, R., et al. 2005, *ApJL*, 631, L13
- Daddi, E., Dickinson, M., Morrison, G., et al. 2007, *ApJ*, 670, 156
- Dale, D. A., & Helou, G. 2002, *ApJ*, 576, 159
- Dey, A., Soifer, B. T., Desai, V., et al. 2008, *ApJ*, 677, 943
- Díaz Tello, J., Donzelli, C., Padilla, N., et al. 2013, *ApJ*, 771, 7
- Dunne, L., Ivison, R. J., Maddox, S., et al. 2009, *MNRAS*, 394, 3
- Elbaz, D., Daddi, E., Le Borgne, D., et al. 2007, *A&A*, 468, 33
- Fang, G.-W., Kong, X., & Wang, M. 2009, *Research in A&A*, 9, 59
- Fang, G., Kong, X., Chen, Y., & Lin, X. 2012, *ApJ*, 751, 109
- Förster Schreiber, N. M., van Dokkum, P. G., Franx, M., et al. 2004, *ApJ*, 616, 40
- Foucaud, S., Almaini, O., Smail, I., et al. 2007, *MNRAS*, 376, L20
- Franx, M., Labbé, I., Rudnick, G., et al. 2003, *ApJL*, 587, L79
- Fumagalli, M., Labbé, I., Patel, S. G., et al. 2014, *ApJ*, 796, 35
- Grazian, A., Fontana, A., Moscardini, L., et al. 2006, *A&A*, 453, 507
- Grogin, N. A., Kocevski, D. D., Faber, S. M., et al. 2011, *ApJS*, 197, 35
- Gronwall, C., Ciardullo, R., Hickey, T., et al. 2007, *ApJ*, 667, 79
- Hasinger, G., Cappelluti, N., Brunner, H., et al. 2007, *ApJS*, 172, 29
- Huang, J.-S., Barmby, P., Fazio, G. G., et al. 2004, *ApJS*, 154, 44
- Huang, J.-S., Faber, S. M., Daddi, E., et al. 2009, *ApJ*, 700, 183

- Huang, J.-S., Faber, S. M., Willmer, C. N. A., et al. 2013, *ApJ*, 766, 21
- Ilbert, O., Salvato, M., Le Floch, E., et al. 2010, *ApJ*, 709, 644
- Ilbert, O., et al. 2013, *A&A*, accepted
- Kajisawa, M., & Yamada, T. 2001, *PASJ*, 53, 833
- Kajisawa, M., & Yamada, T. 2005, *ApJ*, 618, 91
- Kajisawa, M., & Yamada, T. 2006, *ApJ*, 650, 12
- Kajisawa, M., Konishi, M., Suzuki, R., et al. 2006, *PASJ*, 58, 951
- Kajisawa, M., Konishi, M., Ichikawa, T., et al. 2008, *Panoramic Views of Galaxy Formation and Evolution*, 399, 296
- Kajisawa, M., Ichikawa, T., Yamada, T., et al. 2010, *ApJ*, 723, 129
- Kajisawa, M., Ichikawa, T., Yoshikawa, T., et al. 2011, *PASJ*, 63, 403
- Kennicutt, R. C., Jr. 1998, *ARA&A*, 36, 189
- Kim, J.-W., Edge, A. C., Wake, D. A., & Stott, J. P. 2011, *MNRAS*, 410, 241
- Koekemoer, A. M., Faber, S. M., Ferguson, H. C., et al. 2011, *ApJS*, 197, 36
- Kong, X., Daddi, E., Arimoto, N., et al. 2006, *ApJ*, 638, 72
- Kong, X., Fang, G., Arimoto, N., & Wang, M. 2009, *ApJ*, 702, 1458
- Kriek, M., van Dokkum, P. G., Franx, M., et al. 2006, *ApJ*, 645, 44
- Kriek, M., van Dokkum, P. G., Franx, M., et al. 2006, *ApJL*, 649, L71
- Kriek, M., van Dokkum, P. G., Franx, M., et al. 2008, *ApJ*, 677, 219
- Kriek, M., van Dokkum, P. G., Labbé, I., et al. 2009, *ApJ*, 700, 221
- Kriek, M., van Dokkum, P. G., Franx, M., et al. 2009, *ApJL*, 705, L71
- Labbé, I., Franx, M., Rudnick, G., et al. 2003, *AJ*, 125, 1107
- Labbé, I., Huang, J., Franx, M., et al. 2005, *ApJL*, 624, L81
- Lane, K. P., Almaini, O., Foucaud, S., et al. 2007, *MNRAS*, 379, L25
- Lee, B., Giavalisco, M., Williams, C. C., et al. 2013, *ApJ*, 774, 47
- Lilly, S. J., Le Brun, V., Maier, C., et al. 2009, *ApJS*, 184, 218
- Lotz, J. M., Madau, P., Giavalisco, M., et al. 2006, *ApJ*, 636, 592
- Martin, D. C., Fanson, J., Schiminovich, D., et al. 2005, *ApJL*, 619, L1
- McCracken, H. J., Capak, P., Salvato, M., et al. 2010, *ApJ*, 708, 202
- McCracken, H. J., Milvang-Jensen, B., Dunlop, J., et al. 2012, *A&A*, 544, A156
- Muzzin, A., Marchesini, D., Stefanon, M., et al. 2013, *ApJS*, 206, 8
- Muzzin, A., Marchesini, D., Stefanon, M., et al. 2013, *ApJ*, 777, 18
- Pannella, M., Carilli, C. L., Daddi, E., et al. 2009, *ApJL*, 698, L116
- Papovich, C., Dickinson, M., Giavalisco, M., et al. 2005, *ApJ*, 631, 101
- Papovich, C., Moustakas, L. A., Dickinson, M., et al. 2006, *ApJ*, 640, 92
- Patel, S. G., van Dokkum, P. G., Franx, M., et al. 2013, *ApJ*, 766, 15
- Reddy, N. A., Erb, D. K., Steidel, C. C., et al. 2005, *ApJ*, 633, 748
- Rodighiero, G., Daddi, E., Baronchelli, I., et al. 2011, *ApJ*, 739, 40
- Sanders, D. B., Salvato, M., Aussel, H., et al. 2007, *ApJS*, 172, 86
- Schinnerer, E., Smolčić, V., Carilli, C. L., et al. 2007, *ApJS*, 172, 46
- Scoville, N., Abraham, R. G., Aussel, H., et al. 2007, *ApJS*, 172, 38

Shapley, A. E. 2011, *ARA&A*, 49, 525  
 Smail, I., Ivison, R. J., & Blain, A. W. 1997, *ApJL*, 490, L5  
 Speagle, J. S., Steinhardt, C. L., Capak, P. L., & Silverman, J. D. 2014, *ApJS*, 214, 15  
 Steidel, C. C., Giavalisco, M., Pettini, M., et al. 1996, *ApJL*, 462, L17  
 Tadaki, K.-i., Kodama, T., Tanaka, I., et al. 2013, *ApJ*, 778, 114  
 Tadaki, K.-i., Kodama, T., Tanaka, I., et al. 2014, *ApJ*, 780, 77  
 Talia, M., et al. 2013, *A&A*, accepted  
 Taniguchi, Y., Scoville, N., Murayama, T., et al. 2007, *ApJS*, 172, 9  
 Toft, S., van Dokkum, P., Franx, M., et al. 2005, *ApJL*, 624, L9  
 van de Sande, J., Kriek, M., Franx, M., et al. 2013, *ApJ*, 771, 85  
 van Dokkum, P. G., Quadri, R., Marchesini, D., et al. 2006, *ApJL*, 638, L59  
 Wang, T., Huang, J.-S., Faber, S. M., et al. 2012, *ApJ*, 752, 134  
 Webb, T. M. A., van Dokkum, P., Egami, E., et al. 2006, *ApJL*, 636, L17  
 Whitaker, K. E., Franx, M., Leja, J., et al. 2014, *ApJ*, 795, 104  
 Williams, C. C., Giavalisco, M., Cassata, P., et al. 2014, *ApJ*, 780, 1  
 Yan, H., Dickinson, M., Eisenhardt, P. R. M., et al. 2004, *ApJ*, 616, 63  
 Yan, L., Sajina, A., Fadda, D., et al. 2007, *ApJ*, 658, 778